Structural basis for allostery in integrins and binding to fibrinogen-mimetic therapeutics

Tsan Xiao[1], Junichi Takagi[1]*, Barry S. Coller[2], Jia-Huai Wang[3] & Timothy A. Springer[1]

[1]*The CBR Institute for Biomedical Research and Department of Pathology, Harvard Medical School, 200 Longwood Avenue, Boston, Massachusetts 02115, USA*
[2]*Laboratory of Blood and Vascular Biology, The Rockefeller University, 1230 York Avenue, New York, New York 10021, USA*
[3]*Dana-Farber Cancer Institute, Departments of Pediatrics, Biological Chemistry and Molecular Pharmacology, Harvard Medical School, 44 Binney Street, Boston, Massachusetts 02115, USA*

* Present address: Institute for Protein Research, Osaka University, 3-2 Yamadaoka, Suita, Osaka 565-0871, Japan

Integrins are important adhesion receptors in all Metazoa that transmit conformational change bidirectionally across the membrane. Integrin α and β subunits form a head and two long legs in the ectodomain and span the membrane. Here, we define with crystal structures the atomic basis for allosteric regulation of the conformation and affinity for ligand of the integrin ectodomain, and how fibrinogen-mimetic therapeutics bind to platelet integrin $\alpha_{IIb}\beta_3$. Allostery in the β_3 I domain alters three metal binding sites, associated loops and α1- and α7-helices. Piston-like displacement of the α7-helix causes a 62° reorientation between the β_3 I and hybrid domains. Transmission through the rigidly connected plexin/semaphorin/integrin (PSI) domain in the upper β_3 leg causes a 70 Å separation between the knees of the α and β legs. Allostery in the head thus disrupts interaction between the legs in a previously described low-affinity bent integrin conformation, and leg extension positions the high-affinity head far above the cell surface.

Integrins are adhesion receptors that transmit signals bidirectionally across the plasma membrane[1–4]. Rearrangements in integrin extracellular, transmembrane and cytoplasmic domains underlie diverse biological processes, including cell migration, morphogenesis, immune responses and vascular haemostasis. The platelet-specific integrin $\alpha_{IIb}\beta_3$ is important in both the arrest of bleeding at sites of vascular injury and pathological thrombosis leading to heart attacks and stroke. Loss of the vascular endothelium results in platelet deposition, and receptors for collagen, thrombin and other agonists then initiate platelet signalling, resulting in changes in the cytoplasmic domains of $\alpha_{IIb}\beta_3$ that are transmitted into conformational changes in the extracellular domains. This leads to high-affinity binding of fibrinogen and von Willebrand factor, resulting in crosslinking of platelets into aggregates by these multivalent ligands, and activation by $\alpha_{IIb}\beta_3$ of further intracellular signals. Mutations of either α_{IIb} or β_3 result in the bleeding disorder Glanzmann thrombasthenia and drugs that inhibit ligand binding to $\alpha_{IIb}\beta_3$ are effective in preventing and treating coronary artery thrombosis[5].

Global structural rearrangements in integrin extracellular domains are demonstrated by electron microscopy and exposure of activation epitopes known as ligand-induced binding sites (LIBS)[2,4]. Negative stain electron microscopy with image averaging of integrins has demonstrated three overall conformations of the extracellular domain[3,6] (Fig. 1a–c). A low-affinity, bent conformation (Fig. 1a) matches an $\alpha_V\beta_3$ crystal structure[7,8]. An extended form with a 'closed' headpiece conformation matching that in the crystal structure represents an intermediate affinity state (Fig. 1b). Ligand-binding induces a high-affinity, extended form with an 'open' headpiece, in which the angle between the β I and hybrid domains changes from acute to obtuse[3,6] (Fig. 1c). This marked change in tertiary structure is supported by mutational studies[3,6,9–11] and solution X-ray scattering[12]. Ligand-mimetic compounds induce the extended, open headpiece conformation of integrins in solution and on the cell surface[3,6,10–13], and LIBS epitope exposure[14]. In contrast, when a ligand-mimetic is soaked into preformed crystals containing the bent integrin conformation with the closed headpiece, binding induces only localized structural changes near the ligand binding site[8].

In the low-affinity bent structure, the α and β subunit ectodomain carboxy termini[7] and transmembrane domains are closely associated[15,16], and transmission of activation signals across the membrane involves separation between the α and β transmembrane and cytoplasmic domains[16–18]. How allostery could be relayed between the integrin transmembrane domains, legs and ligand-binding head has been unclear. We have proposed that the conformation of the ligand-binding site atop the integrin β I domain could be transmitted to the outward swing of the β hybrid domain between the closed and open headpiece conformations (Fig. 1b, c) by a piston-like β I domain α7-helix motion similar to that seen in integrin α I domains[3,6]. However, in the absence of atomic views of the high-affinity integrin state, different opinions about its conformation have been put forward.

Here, atomic structures of $\alpha_{IIb}\beta_3$ fragments demonstrate the high-affinity, open conformation of the integrin headpiece, its binding to therapeutic antagonists, and the allosteric movements that link the ligand binding site of β I domains to α7-helix displacement and outward swing of the hybrid domain. The β_3 hybrid and PSI domains act as a rigid lever that transmits and amplifies this motion, resulting in a 70 Å separation between the α and β legs at their knees that favours leg extension.

Overall structure of an open integrin headpiece

Two crystal forms each contain α_{IIb} residues 1–452 comprising the β-propeller domain and β_3 residues 1–440 including the β I, hybrid and PSI domains (Fig. 2a, b and Supplementary Table 1). Crystal form A contains one copy per asymmetric unit of the $\alpha_{IIb}\beta_3$ headpiece bound to 10E5 Fab[19] (Fig. 2a), and ligand-mimetic antagonist or cacodylate ion bound to the β_3 I domain metal-ion-dependent adhesion site (MIDAS) (2.7–3.1 Å resolution). Crystal form B contains no Fab and three independent, cacodylate-bound $\alpha_{IIb}\beta_3$ molecules per asymmetric unit (2.9 Å resolution). The four

independent $\alpha_{IIb}\beta_3$ headpiece fragments from the two crystal forms adopt similar conformations, with only minor differences in the angle between the β I and hybrid domains (Fig. 2b). Five N-linked glycans are resolved, including one in a form A crystal lattice contact with seven carbohydrate residues (Fig. 2a). Residues 55–77 in our β_3 hybrid domain structures have a different sequence-structure register than previous β_3 structures (Supplementary Material).

Our crystal structures reveal an open, high-affinity conformation of the $\alpha_{IIb}\beta_3$ headpiece similar to that in electron microscopy averages of the $\alpha_V\beta_3$ ectodomain in which ligand binding induced the extended conformation with the open headpiece[3] (Fig. 1c). Relative to the bent $\alpha_V\beta_3$ crystal structure with the closed, low-affinity conformation of the headpiece[3,7], the α7-helix of the β_3 I domain moves downward, causing the hybrid and PSI domains to swing away from the α subunit by 62° (Fig. 2d). The angle between the β I and hybrid domains visualized here is in excellent agreement with that found by electron microscopy for liganded $\alpha_V\beta_3$ (ref. 3) and the $\alpha_5\beta_1$ headpiece bound to FN3 module 10 of fibronectin[6] (Fig. 2e). Ligand-mimetic antagonists are known to induce the conformation of $\alpha_{IIb}\beta_3$ with high affinity for fibrinogen[14]. Crystallization in the open conformation may also have been facilitated by truncation of the integrin tailpiece, which participates in extensive interfaces that stabilize the bent $\alpha_V\beta_3$ conformation[3]. The conformation characterized here termed 'liganded-open' was obtained by co-crystallization with ligand, enabling equilibration to the most favoured ligand-bound conformation before crystallization. By contrast, crystals of $\alpha_V\beta_3$ were previously formed in the bent, low-affinity conformation which we term 'unliganded-closed', and a ligand-mimetic antagonist was then soaked-in to obtain what we term the 'liganded-closed' conformation[8]. Crystal packing contacts are required for maintenance of the bent, liganded-closed conformation, because in solution addition of the same ligand to bent $\alpha_V\beta_3$ induces leg extension and conversion of the headpiece to the open conformation[3].

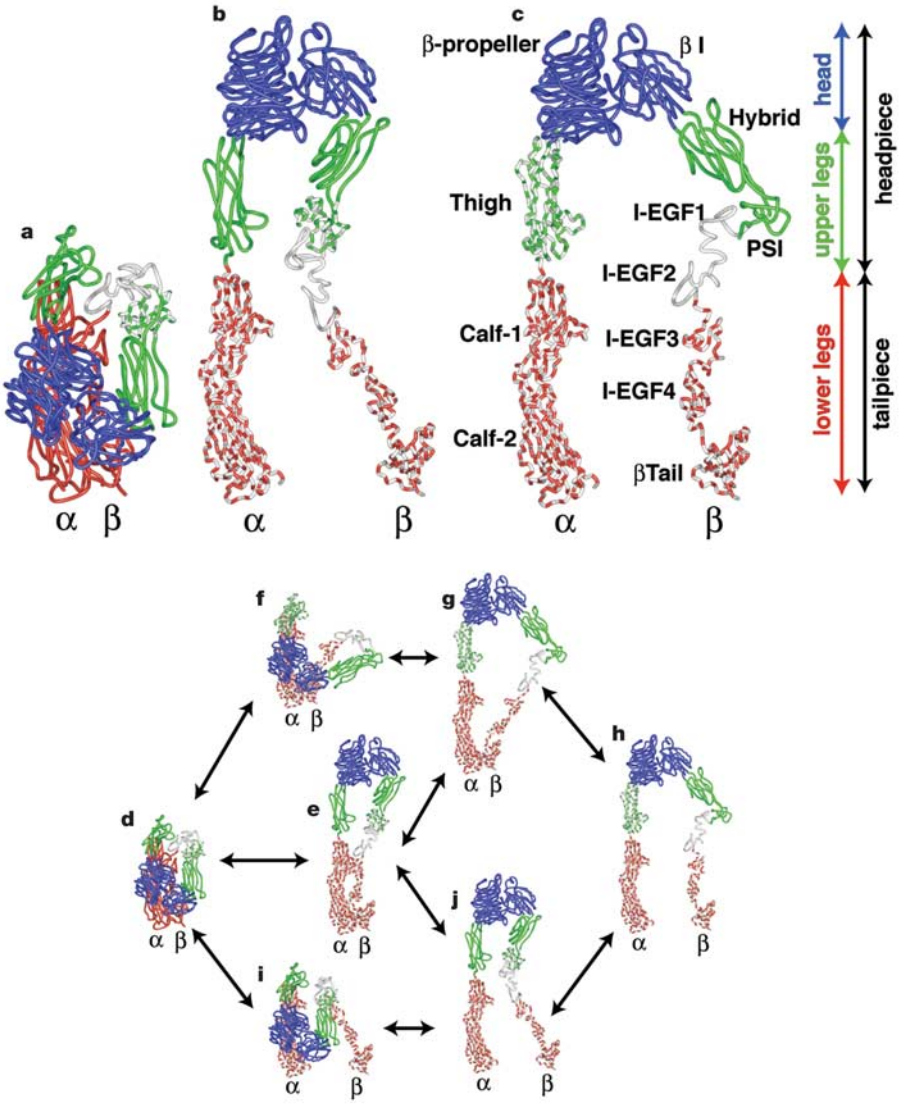

Figure 1 Quaternary rearrangements in the integrin ectodomain. **a**–**c**, Three conformational states visualized in electron microscopy[3,6] and in crystal structures (here and in ref. 7). **d**–**j**, Proposed intermediates in equilibration between known conformational states. The upper pathways may be stimulated by ligand binding outside the cell, and the lower pathways by signals within the cell that separate the α and β subunit transmembrane domains. Domains in **a**–**j** are shown in solid colour if known directly from crystal structures, dashed with grey if placed from crystal structures into electron microscopy image averages, and in solid grey for EGF-1 and EGF-2, which are modelled on EGF-3 and EGF-4.

Ligand binding to $\alpha_{IIb}\beta_3$

Small molecule antagonists bind to a small pocket atop the integrin head formed by loops from the α_{IIb} β-propeller and β_3 I domain (Figs 2a and 3a–d). The binding site for the macromolecular ligand fibrinogen is more extensive, as revealed by the positions of residues shown by mutation to affect binding (Fig. 3a). In macromolecular recognition, the β_3 specificity determining loop (SDL) and four α_{IIb} β-propeller loops that form a cap subdomain are particularly important, with 71% of fibrinogen-sensitive α_{IIb} mutations mapping to the latter[20]. The α_{IIb}-specific 10E5 Fab binds solely to the α_{IIb} cap subdomain (Fig. 2a, Supplementary Material and Supplementary Fig. 2) and has no effect on its conformation (Fig. 2b). Binding of small molecules is not blocked by 10E5, as shown by their co-crystallization (Figs 2a and 3a–d), and thus blocks binding of fibrinogen to $\alpha_{IIb}\beta_3$ (ref. 19) solely by occluding the macromolecular recognition site on the α_{IIb} cap subdomain. By contrast, the β_3 specific-7E3 Fab, abciximab, blocks fibrinogen-binding by binding to residues in the β_3 SDL[5,21].

The cap subdomain helps form the drug-binding pocket as well as the macromolecular recognition surface on α_{IIb}. It is comprised of four long insertions or loops in the β-propeller domain (Supplementary Fig. 1a). Insert 3 forms an α-helix in the α_{IIb} drug-binding pocket (Fig. 3a–d), and in integrin α subunits that contain I domains forms the ligand-binding α I domain[4]. Inserts 1 and 2 form a four-stranded anti-parallel β-sheet in the centre of the cap subdomain that is buttressed on one side by the α-helix and loop of insert 4, and on the other side by the β_3 SDL (Fig. 2a). Alternative splicing of cap insert 4 can regulate ligand-binding specificity[22,23].

The greatest structural differences between the α_{IIb} and α_V β-propellers are in cap inserts 1, 2 and 3 (Fig. 2d). The β_3 SDL closely associates with the cap subdomain, and structural variation between α_{IIb} and α_V appears to be responsible for the different β_3 SDL conformations in $\alpha_{IIb}\beta_3$ and $\alpha_V\beta_3$ (Figs 2d and 3d compared with 3f). By contrast, the remainder of the α_{IIb} and α_V β-propellers

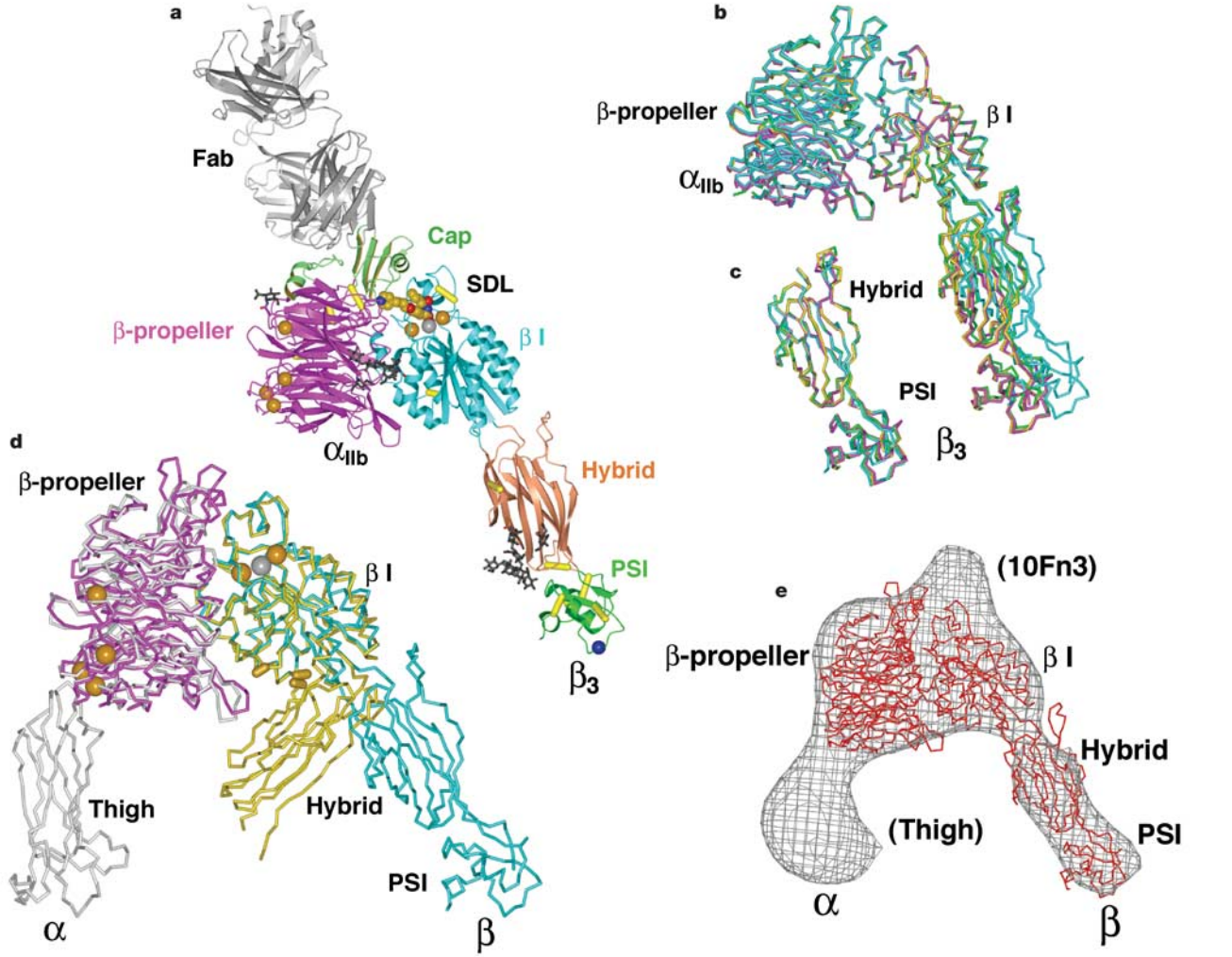

Figure 2 Structure of the $\alpha_{IIb}\beta_3$ headpiece. **a**, Ribbon diagram of the $\alpha_{IIb}\beta_3$:10E5 complex. Calcium and magnesium ions are shown as gold and silver spheres, respectively. Tirofiban is shown in cpk. The Cα atom of HPA-1a alloantigenic determinant Leu 33 in the PSI domain is shown as a blue sphere. Glycan chains are displayed as black sticks. Integrin disulphides are shown as yellow Cα–Cα bonds. **b**, Superimposed on the basis of the β I domain are the three independent $\alpha_{IIb}\beta_3$ heterodimers in crystal form B (magenta, green and yellow), and one in form A (cyan). **c**, The hybrid and PSI domains of the four independent $\alpha_{IIb}\beta_3$ structures are superimposed. **d**, Liganded-open $\alpha_{IIb}\beta_3$ (crystal form A) and unliganded-closed $\alpha_V\beta_3$ headpieces[7] are superimposed using the β I domain β-sheet. The α and β subunits are coloured magenta and cyan in $\alpha_{IIb}\beta_3$ and grey and yellow in $\alpha_V\beta_3$. Calcium and magnesium ions in $\alpha_{IIb}\beta_3$ only are gold and silver spheres, respectively. Yellow cylinders in the β I/hybrid interface show positions of residues where introduction of N-glycosylation sites induces high affinity for ligand and LIBS epitope exposure[9,42]. **e**, Superposition of an $\alpha_{IIb}\beta_3$ structure from crystal form B (red Cα-trace) on the three-dimensional electron microscopy density (grey chickenwire) of the fibronectin-bound $\alpha_5\beta_1$ headpiece[6]. Domains are labelled and those only in the $\alpha_5\beta_1$ structure including the tenth FN3 domain of fibronectin are in parentheses. Figures in this paper utilize crystal form A unless stated otherwise and were prepared with programs Bobscript[46], Povray (The Povray Team, http://www.povray.org), Raster3D[47] and Ribbons[48].

are highly conserved structurally, with a root mean square deviation of 1.4 Å for 391 residues. The hub of the β-propeller that associates with the β I domain is especially conserved, enabling up to eleven diverse integrin α-subunits to bind to a single β-subunit[24]. At their current resolutions of 2.7 Å and 3.1 Å, respectively, there is no significant difference between liganded-open $\alpha_{IIb}\beta_3$ and unliganded-closed $\alpha_V\beta_3$ in orientation between the β-propeller and β I domains (Fig. 2d).

All crystals reported here were formed in the presence of the physiological cations Ca^{2+} and Mg^{2+}. Three metal binding sites are present in the β_3 I domain in the drug-binding pocket[8] (Figs 2a and 3a–f). In the middle site, the MIDAS, a Mg^{2+} ion coordinates a carboxyl group present in each of the three co-crystallized ligand-mimetic $\alpha_{IIb}\beta_3$ antagonists (Fig. 3a–d). The cacodylate ion that is bound to form A (Fig. 3e) and form B crystals binds in the same way as the carboxyl group of the ligand-mimetics, with one oxygen coordinating the MIDAS Mg^{2+} and the other hydrogen-bonding to two backbone amides. The cacodylate may thus act as a pseudo-ligand, and stabilize the open β subunit I domain conformation similarly to pseudoligand lattice contacts that stabilize the open α subunit I domain conformation[25–27]. Ca^{2+} was assigned at the two sites adjacent to the MIDAS on the basis of Yb^{3+} soaking data and coordination chemistry (see Methods). The site distal to the β-propeller is termed adjacent to MIDAS (ADMIDAS). The site near the β-propeller is termed ligand-induced metal binding site (LIMBS). The LIMBS is occupied in the open $\alpha_{IIb}\beta_3$ structure even when only a cacodylate pseudoligand is bound (Fig. 3e).

Two drugs used in prevention and treatment of coronary artery thrombosis, tirofiban and eptifibatide[5], as well as Merck compound L-739758 (Fig. 3a–d), antagonize binding of fibrinogen to $\alpha_{IIb}\beta_3$. These compounds were developed as mimics of the Arg-Gly-Asp sequence that is found in a wide variety of integrin glycoprotein

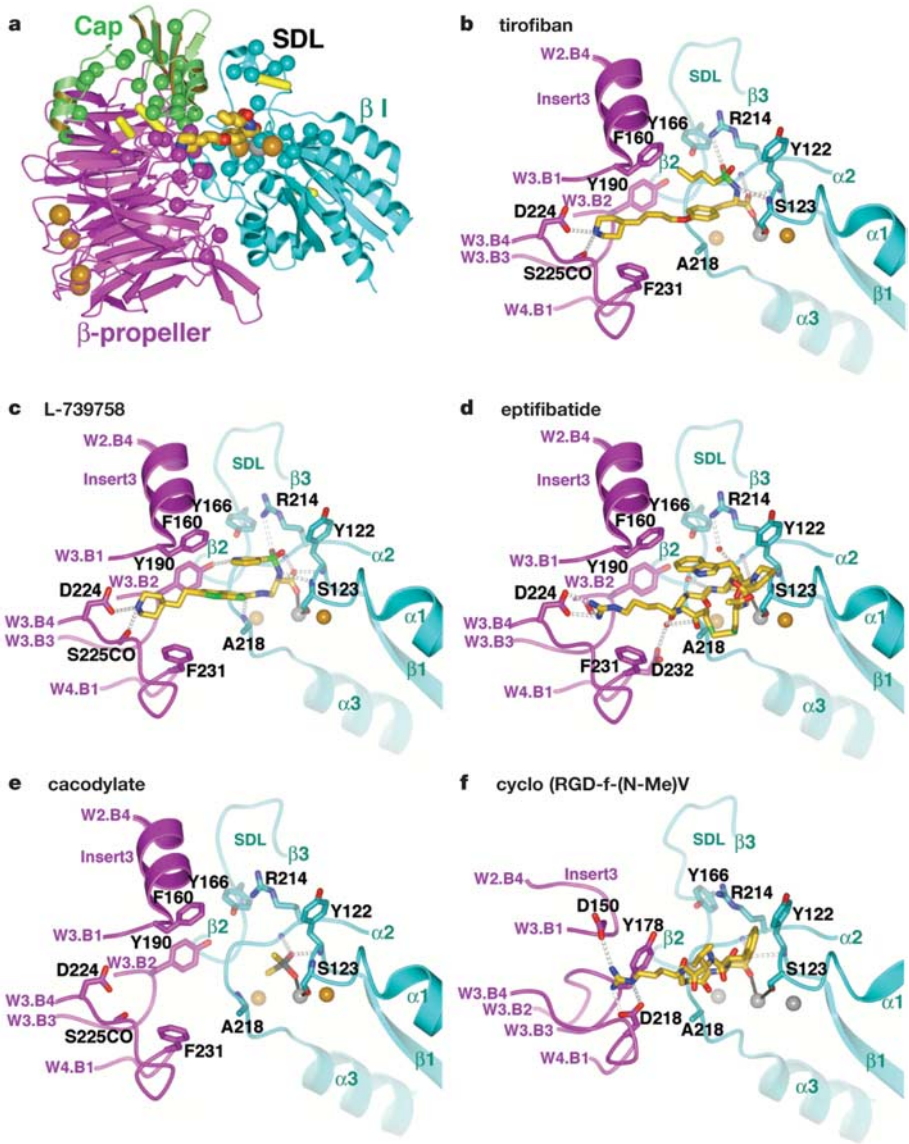

Figure 3 The binding sites for ligand-mimetic antagonists and fibrinogen at the α/β subunit interface. **a**, Mapping of fibrinogen binding sensitive mutations[20,49,50] in $\alpha_{IIb}\beta_3$. Cβ atoms of fibrinogen-binding sensitive residues are shown as spheres in the same colour as the domains in which they are present. The tirofiban-bound structure is shown. **b**–**f**, Binding of ligands or pseudoligands to $\alpha_{IIb}\beta_3$ (**b**–**e**) and binding of (**f**) cyclo Arg-Gly-Asp-D-Phe-N-methyl-Val (cyclo RGDfV) to $\alpha_V\beta_3$ (ref. 8). The orientation is identical to that in **a**. The α and β subunits are shown in magenta and cyan, respectively. Small molecules are shown as ball-and-stick models with their carbon, nitrogen, oxygen, sulphur and arsenic atoms coloured yellow, blue, red, green and grey, respectively. Hydrogen bonds are shown as dotted lines. Ca^{2+} and Mg^{2+} ions are gold and silver spheres, respectively. The ligand and S123 coordinations to the MIDAS metal are shown as thin grey lines.

ligands, and the $\alpha_{IIb}\beta_3$-binding sequence in fibrinogen, Lys-Gln-Ala-Gly-Asp-Val[28,29,30]. In addition to $\alpha_{IIb}\beta_3$, the integrins $\alpha_V\beta_1$, $\alpha_V\beta_3$, $\alpha_V\beta_5$, $\alpha_V\beta_6$, $\alpha_V\beta_8$, $\alpha_5\beta_1$ and $\alpha_8\beta_1$ recognize the Arg-Gly-Asp motif. Therefore, a major focus of pharmaceutical development was selective inhibition of $\alpha_{IIb}\beta_3$, particularly in comparison to the closely related $\alpha_V\beta_3$ integrin. Our co-crystal structures (Fig. 3b–d), and comparison to an $\alpha_V\beta_3$-selective compound soaked into $\alpha_V\beta_3$ crystals (Fig. 3f)[8], reveal the basis for drug binding and selectivity (see Supplementary Material for details). Each drug has a basic moiety that mimics the arginine in Arg-Gly-Asp or the lysine in the fibrinogen sequence, and a carboxyl group that mimics the aspartic acid. Selectivity for $\alpha_{IIb}\beta_3$ and $\alpha_V\beta_3$ is conferred by a longer and shorter distance, respectively, between the basic and acidic moieties of peptidomimetics (Fig. 3d, f), which can be adjusted by the constraints on the cyclic ring that bears the basic and aspartic acid residues, and the length of the basic residue side chain[28,29]. Our structures show that this is because the basic ligand-mimetic side chain must reach further into the deeper β-propeller pocket of α_{IIb} to hydrogen-bond to α_{IIb}-Asp 224 (Fig. 3b–d), whereas in the α_V β-propeller the hydrogen-bonding residues Asp 150 and Asp 218 are nearer in its shallower pocket (Fig. 3f). Furthermore, Asp 218 in α_V is replaced by Phe 231 in α_{IIb}, favouring contacts with longer aliphatic moieties (Fig. 3b–d, f).

A large number of snake venom disintegrins with Arg-Gly-Asp sequences have evolved to inhibit haemostasis but are not $\alpha_{IIb}\beta_3$-selective. An unusual, $\alpha_{IIb}\beta_3$-selective disintegrin with a Lys-Gly-

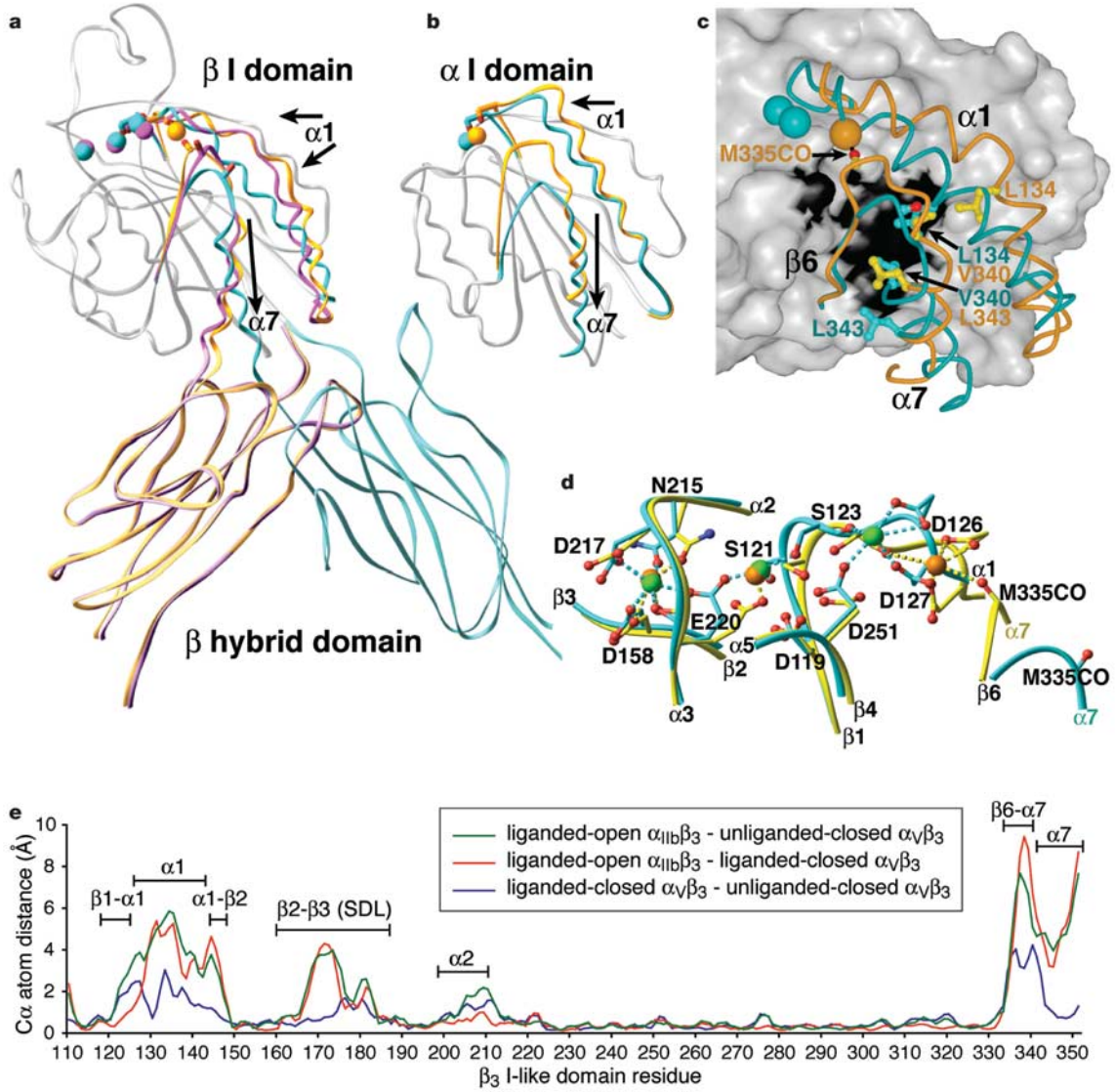

Figure 4 Allostery in the β I domain and comparison with α I domain. **a**, Overview of motions in the β_3 I and hybrid domains. Non-moving parts of the backbone are shown as a grey worm. Moving segments shown as Cα-traces are from unliganded-closed $\alpha_V\beta_3$ (gold), liganded-closed $\alpha_V\beta_3$ (magenta) and liganded-open $\alpha_{IIb}\beta_3$ (cyan). The direction of movement is shown with arrows. **b**, Comparison with α I domains. The moving segments of unliganded-closed (gold) and pseudoliganded-open (cyan) α_M I domains[25,26] and their MIDAS metal ions are shown as in **a** and in the same orientation. **c**, Hydrophobic ratchet pockets underlying the β6–α7 loop and α1-helix. The unliganded-closed (orange) and liganded open (cyan) β1–α1 loop, α1-helix, α1–β2 loop and β6–α7 loop and α7-helix are shown as worm traces with key side chains, the Met 335 carbonyl and metal ions in the same colour. The rest of the domain is shown as a grey surface, except for hydrophobic pocket residues Tyr 116, Val 247, Thr 249, Ile 307, Ala 309 and Thr 311, which are shown as a black surface. **d**, β_3 I domain metal coordination sites in liganded-open $\alpha_{IIb}\beta_3$ (cyan) and unliganded-closed $\alpha_V\beta_3$ (yellow). LIMBS, MIDAS and ADMIDAS positions are shown left to right in similar orientation as in **a**. The LIMBS and MIDAS were not occupied in the unliganded-closed structure[7]; for reference, metal ions at these sites are shown from the liganded-closed structure[8]. In **a**–**d**, metal ions are shown as spheres in the same or a similar (**d**) colour as their associated backbone. **e**, Distances between Cα atoms in the three superimposed β I domains, smoothed by averaging at each residue over a 3-residue window.

Asp-Trp sequence led to the development of eptifibatide[31]. The lysine with its longer aliphatic side chain than arginine confers selectivity, whereas the tryptophan confers high affinity. In an independent drug development programme, exosite substituents such as pyridyl sulphonamide were found that substantially increase affinity[30] (Fig. 3c) and that occupy the same position in the drug-binding pocket as the tryptophan residue (Fig. 3d).

Comparison to the cacodylate-bound structure (Fig. 3e) demonstrates that the drug-binding pocket in $\alpha_{IIb}\beta_3$ is rigid, with the contacting residues adopting the same conformation with or without the drugs. This helps account for high affinity, despite burial of a solvent-accessible surface area of only 300–390 Å^2 on the three drugs.

An open, high-affinity conformation for integrin β I domains

Comparisons among unliganded-closed $\alpha_V\beta_3$, liganded-closed $\alpha_V\beta_3$ and liganded-open $\alpha_{IIb}\beta_3$ reveal the atomic basis for communication of allostery between the ligand binding site in the β_3 I domain and other integrin domains (Figs 2d and 4a, c, d, e; Supplementary Movie 1). In liganded-open $\alpha_{IIb}\beta_3$ compared with unliganded-closed $\alpha_V\beta_3$, concerted movements in the β_3 I domain occur in the ligand-binding β1–α1 loop, the α1-helix, the α1–β2 loop, the α2-helix, the β6–α7 loop and the α7-helix. Movements in the ligand- and metal-binding β1–α1 loop are similar in both liganded structures, but greater in magnitude for the liganded-open structure than the liganded-closed structure (2.9 and 2.0 Å per residue for residues 121–127, respectively) (Fig. 4a, e). A single turn

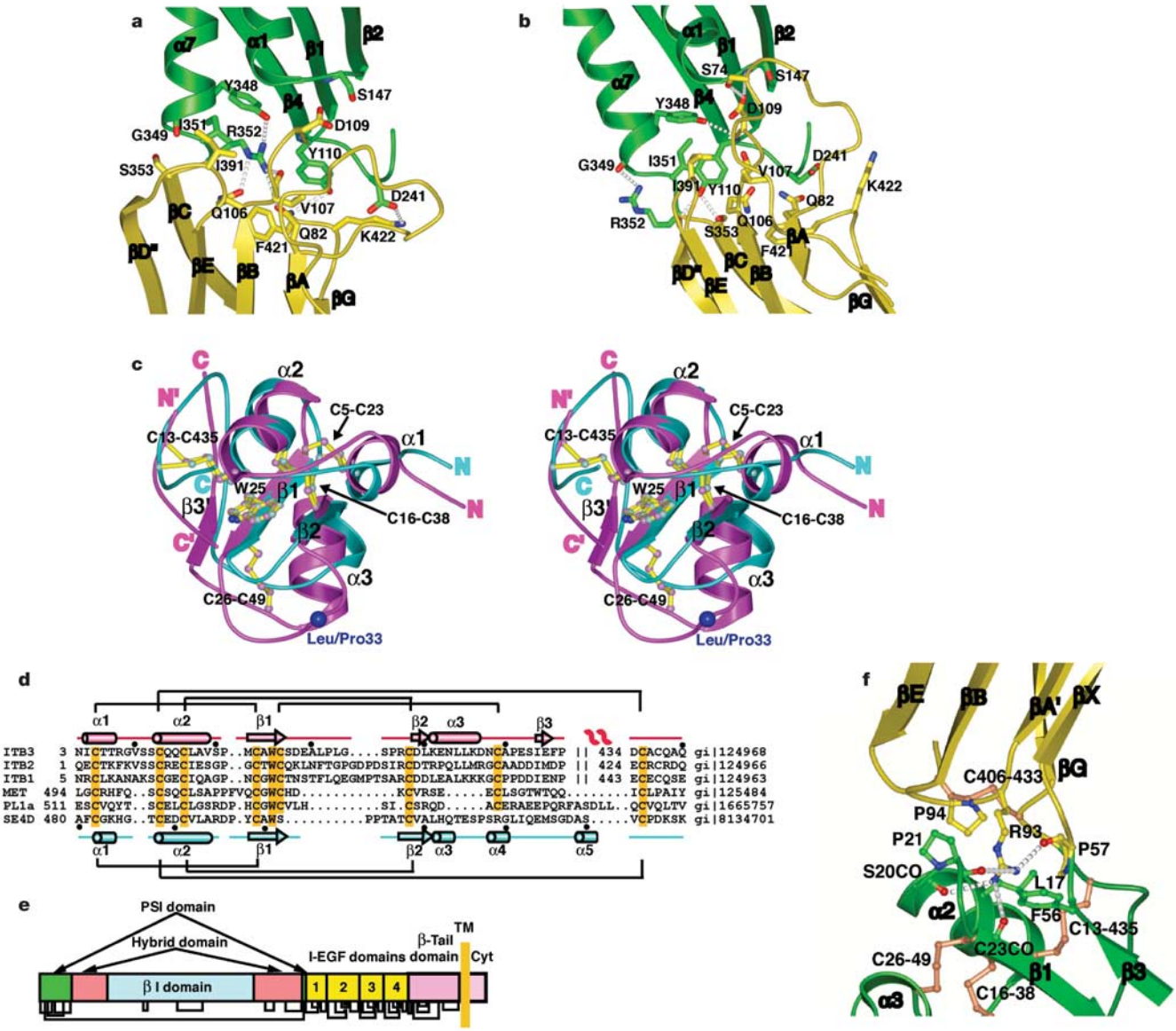

Figure 5 The hybrid and PSI domains and their interfaces. **a**, **b**, The β I/hybrid domain interface in the unliganded-closed structure[7] (**a**) and liganded-open structure (**b**). Ribbon backbone and side-chain carbon atoms are shown in green (β I) and yellow (hybrid) with the β I domain β-sheet in the same orientation. The α7-helical ribbon is shown up to the same residue (350) in both structures to aid comparison of α7-helix position. **c**, Stereo view of the superposition of the PSI domains from β_3 (magenta) and semaphorin4D (cyan). The disulphide bridges and the conserved tryptophan are shown as ball-and-stick models with their bonds coloured yellow and atoms the same colour as the backbone. The Leu/Pro 33 alloantigen site is represented with a large blue Cα sphere. The amino and carboxyl termini of each domain are indicated. The N′ and C′ refer to termini for residues 434–440 that constitute part of the PSI and EGF-1 domains. **d**, Sequence alignment of PSI domains from integrins, semaphorin4D (SE4D), a plexin and c-met. Disulphide connections are shown above (β_3) and below (semaphorin4D) the respective sequences. The conserved cysteines and tryptophans are highlighted orange. The secondary structures are shown for β_3 (top) and sema4D (bottom). **e**, Domain organization of integrin β subunits, showing multiple domain insertions. The revised disulphide bond pattern is shown below. **f**, The interface between the hybrid (yellow) and PSI (green) domains. Disulphide bonds are shown in orange.

of 3_{10}-helix in this loop bearing the key MIDAS and ADMIDAS residue Ser 123 moves *en bloc* in the liganded-open structure, but the lesser movement in the liganded-closed structure disrupts this 3_{10}-helix.

Extensive movements occur in the β6–α7 loop and the α7-helix between the liganded-open and unliganded-closed structures. The β6–α7 loop moves downward, and the α7-helix moves downward and pivots laterally, resulting in an average displacement for residues 333–352 of 5.3 Å (Fig. 4a, c, e). Between the unliganded-closed and liganded-closed structures there is a movement of lesser magnitude in the β6–α7 loop; however, the movements differ in direction (Fig. 4a, e). Movement in this region of the liganded-closed structure is therefore a consequence of strain rather than movement along the pathway towards the open conformation.

In the liganded-open compared with the unliganded-closed structure, the α1-helix moves[32] upward to accommodate movements near its beginning at the MIDAS and ADMIDAS, and near its end, that allow hybrid domain swing-out (Fig. 4a). Furthermore, a bend between the 3_{10}-helix in the β1–α1 loop and the α1-helix is straightened, and the α1-helix is lengthened by five residues, as it pivots laterally to fill-in room vacated by the β6–α7 loop (Fig. 4a, c). The position of the α1-helix in the liganded-closed structure does not resemble that in the unliganded-closed or the liganded-open structures (Fig. 4a, e), suggesting that its position is off the pathway towards the open conformation, and results from strain imposed by binding to ligand when the interface with the hybrid domain remains in the closed conformation.

Changes in metal ion coordination are closely related to loop movements in the β I domain, and are key for stabilizing its alternative conformational states (Fig. 4d). Coordination of the Met 335 backbone carbonyl in the β6–α7 loop to the ADMIDAS Ca^{2+} ion in the unliganded-closed conformation (Fig. 4d)[7] is broken in liganded-closed and Mn^{2+}-bound-closed $\alpha_V\beta_3$[8], and in liganded-open $\alpha_{IIb}\beta_3$ (Fig. 4d). Mn^{2+} activates integrins by competing with Ca^{2+} at the ADMIDAS; the much lower propensity of Mn^{2+} than Ca^{2+} for carbonyl coordination enables downward displacement of the β6–α7 loop and activation in Mn^{2+} (ref. 33). Breakage of the Met 335 coordination and the movement of the β1–α1 loop with its coordinating residues enable the large movement in position of the ADMIDAS metal between the unliganded-closed and liganded-open conformations (Fig. 4d). Additionally, small shifts in the position of the MIDAS and LIMBS metals relate to marked movements and changes in metal ion coordination of residues Asp 251, Glu 220, Asn 215 and Asp 217 (Fig. 4d). The metal ions seem to occupy similar but less strained orientations in the liganded-open compared with the liganded-closed structures, with the caveat that the resolutions are 2.7 and 3.3 Å, respectively. For example, the Asp 217 side chain coordinates with the LIMBS metal ion in the liganded-open structure, instead of orienting away from it in the liganded-closed structure[8,33] (Fig. 4d). Its position in the liganded-open structure is more consistent with the function of Asp 217 in β7 as a LIMBS residue that stabilizes the high-affinity state[33].

Rearrangements in the β I domain are clearly structurally homologous to those in α I domains (Fig. 4a, b). Movements of similar directionality occur in the MIDAS metal ion, β1–α1 loop, α1-helix, β6–α7 loop and α7-helix[4]. Hydrophobic ratchet residues that are located one turn of 3_{10}-helix apart, stabilize alternative β6–α7 loop positions in both α I and β I domains. In contrast to the one-turn displacement in the intermediate[27] and two-turn displacement in the open α I domain conformations[25,26] (Fig. 4b), a one-turn displacement occurs in the open β I domain conformation (Fig. 4a, c). Val 340, located in an upper hydrophobic pocket in the closed conformation, moves to a lower hydrophobic pocket in the open conformation, displacing Leu 343 (Fig. 4c). Movement of the α1-helix plays a similar part in activation of α I and β I domains by accompanying the movement of metal-coordinating residues in the β1–α1 loop; however, the greater magnitude of α1-helix movement in the β I domain is accompanied by a unique ratchet-like movement: residue Leu 134 in the α1-helix moves laterally to occupy the upper hydrophobic pocket vacated by Val 340 (Fig. 4b).

Hybrid domain swing-out

The piston-like displacement of the βI domain α7-helix, which connects to the hybrid domain βC strand, results in complete remodelling of the interface between these domains (Figs 4a and 5a, b; Supplementary Movie 1). The interface in the closed conformation covers 1,350 $Å^2$ and includes at its centre hydrogen-bonding residues Tyr 110, Tyr 348 and Arg 352[7]. Upon opening not only does the α7-helix move downward, but the last two residues unwrap from the helix, including Arg 352, which reorients to the exterior of the interface. The more extended conformation at the junction between α7 and βC, and the straightening of the angle between α7 and βC, augment the effect of α7 displacement on hybrid domain swing-out. The more extended, end-to-end orientation between the β I and hybrid domains results in a smaller interface of about 800 $Å^2$ (Figs 4a and 5a, b). Near its centre the interface contains Tyr 110 and Tyr 348, which adopt new hydrogen-bonding partners (Fig. 5b). Reorganization of hydrogen-bonded interfaces is the general mechanism for allosteric transitions[34]. The smaller size of the open β I/hybrid interface allows some flexibility. Relative to the closed conformation, the hybrid domain swings out 69° in crystal form A, and 57°, 59° and 61° in the three molecules in crystal form B (Fig. 2b).

Structure of an integrin PSI domain

The structure of a PSI domain in an integrin (Fig. 2a and Supplementary Fig. 3b) and comparison to that in semaphorin 4D[35] demonstrate the predicted homology of these domains in plexins, semaphorins and integrins[36], and an unexpected insertion. The buried β1 strand bearing the invariant tryptophan, and the disulphide-bonded α1- and α2-helices are well conserved, but other regions differ significantly, including the longer α3-helix (Fig. 5c, d). All three shared disulphide bonds superimpose well, and a fourth shared with integrins, plexins and the growth factor receptor MET, but not semaphorins, is also revealed (Fig. 5c, d). Chemical assignment of disulphides in the integrin β_3 PSI domain was difficult because cysteines are so closely spaced in sequence[37]; the structural data reassigns all of these disulphides, including the long-range disulphide, which was previously identified as Cys 5 to Cys 435, and is now shown to link Cys 13 to Cys 435 (Fig. 5d, e and Supplementary Fig. 3b). The long-range disulphide superimposes well with the highly conserved intradomain disulphide that links the second cysteine to the last cysteine in the PSI domain of plexins and semaphorins (Fig. 5c), and this second cysteine aligns perfectly in all PSI domains, maintaining its relationship to the third cysteine in the conserved α2-helix (Fig. 5d). These findings suggest that β_3 Cys 435 is the eighth cysteine of the PSI domain, and an integral part of the PSI domain fold. Therefore, there seems to be a nested domain insertion in the β_3 structure: the β I domain is inserted in the hybrid domain, which is in turn inserted in the PSI domain (Fig. 5e).

Superposition of four independent molecules shows that the 860 $Å^2$ interface between the hybrid and PSI domain is rigid (Fig. 2c). Arg 93 of the hybrid domain, which is invariant in vertebrate integrins, inserts its side chain into the centre of the interface, making hydrogen bonds to one hybrid domain residue and three different PSI domain residues (Fig. 5f). Rigidity of the interface is further supported by the nearby Cys 13-Cys 435, Cys 16-Cys 38 and Cys 26-Cys49 disulphides in the PSI domain, and the Cys 406-Cys 433 disulphide in the hybrid domain (Fig. 5f). The connection to integrin EGF-like (I-EGF) domain 1 may also be rigid, because a portion of it containing residues 437–440, including

Cys 437 that is predicted to be disulphide-linked within I-EGF1[38], is present in the structure and stabilized by main-chain–side-chain and side-chain–side-chain hydrogen bonds with the PSI domain.

The human platelet alloantigen HPA-1 or Pl^A system, of great importance for neonatal alloimmune thrombocytopenia and post-transfusion purpura, corresponds to a leucine/proline polymorphism at PSI residue 33 (ref. 39). Our structure shows that the Leu 33 side chain is well exposed to solvent (Fig. 2a) on a loop of the PSI domain that is flexible and particularly long in integrins (Fig. 5c, d). Polymorphic substitution of the distally located residue Arg 93 at the hybrid/PSI interface (Fig. 5f) disrupts the HPA-1a epitope[40], demonstrating the importance of the interface for structural integrity of the PSI domain. The I-EGF1 domain also participates in the HPA-1 epitope[41], further emphasizing the tight linkage between the hybrid, PSI and I-EGF1 domains.

Allosteric mechanism for integrin activation

The structural rearrangements demonstrated here between the closed and open conformations seem to be general for all integrins. The effects of mutations designed to induce hybrid domain swing-out[9,42] (Fig. 2d), allosteric activating or inhibitory mAb that bind to the hybrid domain[10,13] (Supplementary Fig. 4), disulphide cross-links in the β6–α7 loop[43] and shortening of the α7-helix in the β I domain[44], all support the conclusion that the closed and open conformations of the integrin headpiece have low and high affinity for ligand, respectively. Furthermore, these experiments have been conducted on β_1, β_2, β_3 and β_7 integrins, demonstrating the generality of our findings. Moreover, the structural rearrangements shown here are consistent with exposure of LIBS and activation epitopes, including on the PSI domain in models of the complete integrin ectodomain (Supplementary Materials).

Our study reveals the β I/hybrid domain interface as the epicentre for quaternary structural rearrangements in integrins. A movement of about 10 Å occurs at the junction between the β I domain α7-helix and the hybrid domain βC-strand that results in a 62° pivot at the β I/hybrid domain interface. The rigidly connected hybrid and PSI domains act as a mechanical lever in the upper β leg that amplifies and transmits β I domain allostery to the knee between the upper and lower β legs, resulting in a 70 Å displacement at the PSI domain. Because the PSI domain is near the β knee between I-EGF1 and I-EGF2, and in the closed conformation of the headpiece the β knee is near the α subunit knee or genu, the two legs must separate by about 70 Å at their knees (Fig. 1b, c). Swing-out of the upper β leg could readily occur if it were preceded by extension at the α and β knees (Fig. 1d to 1e to 1g). Electron microscopy studies show that below the PSI domain, the β leg is flexible in the extended conformation, whereas when the α leg extends, it adopts a single favoured orientation[3]. Interestingly, swing-out of the upper β leg might also occur in the bent conformation (Fig. 1d to 1f), because if the β subunit upper and lower legs moved as a rigid body, there would be no clash with the α subunit, facilitating conformational equilibration, and despite the 70 Å separation at the knees, the C termini of the α and β subunit ectodomains would only move apart by 15 Å. Thus, adjustments in the flexible β subunit lower leg domains could allow the α and β subunit transmembrane domains to remain associated during upper leg swing-out in the bent conformation (Fig. 1d to 1f to 1g). Transmembrane domain separation could thus occur as a later event in the process of integrin activation by ligand from outside the cell (Fig. 1g to 1h), whereas transmembrane domain separation is a key early step in activation by signals from within the cell[3,16] (Fig. 1d to 1e to 1j to 1h, or Fig. 1d to 1i to 1j to 1h). In the bent $\alpha_V\beta_3$ integrin conformation, there are large, hydrophilic interfaces of 2,000 $Å^2$ each between the headpiece and the legs, and between the α and β subunit legs[3]. The latter interface would be disrupted by upper β leg swing-out, thereby weakening that between the headpiece and the legs, and facilitating adoption of the extended integrin conformation with the open headpiece observed for liganded integrins by electron microscopy[3,6] (Fig. 1c and 1h).

Our crystal structures, together with previous structural studies on integrins[3,6–8,12,15,38], now provide a clear picture of the conformational rearrangements in the integrin head that regulate affinity for ligand, and how conformational signals are transmitted to the leg domains. Further structures are needed to define I-EGF domains 1 and 2 in both the bent and extended conformations, the apparently unique conformation of the α subunit genu in the extended conformation[3], and how allostery is communicated between the β I and α I domains[4]. □

Methods

Protein expression, purification and crystallization

For details and references, see Supplementary Materials. Briefly, the soluble $\alpha_{IIb}\beta_3$ headpiece encompassing residues 1–621 of α_{IIb} and residues 1–472 of β_3 was expressed in CHO Lec 3.2.8.1 cells with an ACID-BASE coiled-coil clasp at the C termini, as described for soluble $\alpha_5\beta_1$[45], except that a hexahistidine tag was fused to the C terminus of β_3. The expressed protein was purified by ammonium sulphate precipitation, Ni-NTA affinity chromatography and size exclusion chromatography (Superdex 200 HR), concentrated to 1 mg ml^{-1}, and treated with chymotrypsin at 25 °C for 16 h. The unclasped (coiled-coil and His_6 tag removed) $\alpha_{IIb}\beta_3$ protein was collected in the flow-through of a second Ni-NTA chromatography step. The purified $\alpha_{IIb}\beta_3$ was mixed with the 10E5 Fab (1:1.1 molar ratio) and the complex was purified by Superdex 200 chromatography. The complex was subjected to digestion with carboxypeptidase A and B (Calbiochem) (1:100 weight ratio) in the presence of 1 mM $ZnCl_2$ at 25 °C for 16 h. A stable protease resistant core of $\alpha_{IIb}\beta_3$ was obtained and further purified by a final Superdex 200 chromatography step and stored in TBS plus calcium and magnesium, and used to obtain crystal form A. To obtain crystal form B, $\alpha_{IIb}\beta_3$ fragment purified through the second Ni-NTA chromatography step was mixed with an excess of the purified fibrinogen γ chain C-terminal domain fragment (see Supplementary Information) in the presence of 1 mM $MnCl_2$ and subjected to carboxypeptidase A and B treatment. This resulted in the same pattern of $\alpha_{IIb}\beta_3$ digestion as for the 10E5 Fab complex sample; however, little of the fibrinogen domain co-purified with the $\alpha_{IIb}\beta_3$ headpiece upon Superdex 200 chromatography, probably owing to hydrolysis of the $\alpha_{IIb}\beta_3$-binding C-terminal residues of the fibrinogen γ chain by carboxypeptidase. This material was used to obtain crystal form B, which contains no fibrinogen fragment.

The Topaz crystallizer (Fluidigm) was used to identify initial crystallization conditions by free interfacial diffusion and the lead conditions were optimized with hanging-drop vapour diffusion. The final optimized well solution for form A crystals of the 10E5 Fab: $\alpha_{IIb}\beta_3$ complex is 11% PEG 3350, 0.7 M magnesium acetate and 0.1 M sodium cacodylate, pH 6.5, and for crystal form B is 10% PEG 8000, 0.4 M magnesium acetate and 0.1 M sodium cacodylate, pH 7.0. Acetate and 4 °C temperature were absolutely required for crystallization. To obtain co-crystals with the drugs, protein sample was mixed with each drug at 1:3 to 1:5 molar ratios before setting up the hanging drops. The optimized crystallization conditions were 10–12% PEG 3350, 0.7 M magnesium acetate and 0.1 M imidazole (pH 6.5) in place of cacodylate.

Structure determination

Diffraction data were collected at the 19-ID station of the Advanced Photon Source (APS) at the Argonne National Laboratory and the A-1 station of the Cornell High Energy Synchrotron Source (CHESS). The structure of crystal form A was determined by molecular replacement using search models of the β I domain and the β I domain plus the β-propeller from $\alpha_V\beta_3$ (PDB ID 1L5G), and a murine Fab 36–71 (PDB ID 6FAB). Electron density maps calculated using phases from the search models clearly showed the presence of the hybrid domain, plus difference densities in the CDR loops of the Fab. The hybrid domain was placed in density and rebuilt. Excellent densities for landmark residues Phe 56, Pro 57, Pro 68 and Leu 69 in the first β-strand of the hybrid domain and multiple nearby disulphide bonds in the hybrid and PSI domains (Fig. 5f and Supplementary Fig. 3a) necessitated a change in the sequence-to-structure register of this β-strand. The structure of the PSI domain was built on the basis of the electron density maps computed with refined models and guided by the secondary structure arrangements in the sema4D crystal structure[35]. Strong electron density for the conserved disulphides, the single tryptophan and the secondary structures allowed unambiguous tracing of the whole domain. Continuous electron density extends beyond residue Cys 435 and allowed the building of residues Ala 436 to Gln 440 of I-EGF1, although alternative conformations of these residues cannot be ruled out. The structure of crystal form B was solved by molecular replacement using the $\alpha_{IIb}\beta_3$ structure in crystal form A as a search model. The structures of the drug bound $\alpha_{IIb}\beta_3$ were solved by molecular replacement using the native structure as a search model. Electron density for the bound drug molecules was readily discernible in the maps calculated with the molecular replacement solution.

Received 25 June; accepted 26 August 2004; doi:10.1038/nature02976.
Published online 19 September 2004; corrected 6 October 2004 (see full text online).

1. Hughes, P. E. & Pfaff, M. Integrin affinity modulation. *Trends Cell Biol.* **8,** 359–364 (1998).
2. Takagi, J. & Springer, T. A. Integrin activation and structural rearrangement. *Immunol. Rev.* **186,** 141–163 (2002).
3. Takagi, J., Petre, B. M., Walz, T. & Springer, T. A. Global conformational rearrangements in integrin extracellular domains in outside-in and inside-out signaling. *Cell* **110,** 599–611 (2002).

4. Springer, T. A. & Wang, J.-h. in *Cell Surface Receptors* (ed. Garcia, K. C.) (Elsevier, San Diego, 2004).
5. Coller, B. S. Platelet GPIIb/IIIa antagonists: the first anti-integrin receptor therapeutics. *J. Clin. Invest.* **99,** 1467–1471 (1997).
6. Takagi, J., Strokovich, K., Springer, T. A. & Walz, T. Structure of integrin α5β1 in complex with fibronectin. *EMBO J.* **22,** 4607–4615 (2003).
7. Xiong, J.-P. *et al.* Crystal structure of the extracellular segment of integrin αVβ3. *Science* **294,** 339–345 (2001).
8. Xiong, J. P. *et al.* Crystal structure of the extracellular segment of integrin αVβ3 in complex with an Arg-Gly-Asp ligand. *Science* **296,** 151–155 (2002).
9. Luo, B.-H., Springer, T. A. & Takagi, J. Stabilizing the open conformation of the integrin headpiece with a glycan wedge increases affinity for ligand. *Proc. Natl Acad. Sci. USA* **100,** 2403–2408 (2003).
10. Luo, B.-H., Strokovich, K., Walz, T., Springer, T. A. & Takagi, J. Allosteric β1 integrin antibodies that stabilize the low affinity state by preventing the swing-out of the hybrid domain. *J. Biol. Chem.* **279,** 27466–27471 (2004).
11. Luo, B.-H., Springer, T. A. & Takagi, J. High affinity ligand binding by integrins does not involve head separation. *J. Biol. Chem.* **278,** 17185–17189 (2003).
12. Mould, A. P. *et al.* Structure of an integrin-ligand complex deduced from solution X-ray scattering and site-directed mutagenesis. *J. Biol. Chem.* **278,** 39993–39999 (2003).
13. Mould, A. P. *et al.* Conformational changes in the integrin βA domain provide a mechanism for signal transduction via hybrid domain movement. *J. Biol. Chem.* **278,** 17028–17035 (2003).
14. Du, X. *et al.* Ligands "activate" integrin αIIbβ3 (platelet GPIIb-IIIa). *Cell* **65,** 409–416 (1991).
15. Adair, B. D. & Yeager, M. Three-dimensional model of the human platelet integrin αIIbβ3 based on electron cryomicroscopy and X-ray crystallography. *Proc. Natl Acad. Sci. USA* **99,** 14059–14064 (2002).
16. Luo, B.-H., Springer, T. A. & Takagi, J. A specific interface between integrin transmembrane helices and affinity for ligand. *PLoS Biol.* **2,** 776–786 (2004).
17. Vinogradova, O. *et al.* A structural mechanism of integrin $\alpha_{IIb}\beta_3$ "inside-out" activation as regulated by its cytoplasmic face. *Cell* **110,** 587–597 (2002).
18. Kim, M., Carman, C. V. & Springer, T. A. Bidirectional transmembrane signaling by cytoplasmic domain separation in integrins. *Science* **301,** 1720–1725 (2003).
19. Coller, B. S., Peerschke, E. I., Scudder, L. E. & Sullivan, C. A. A murine monoclonal antibody that completely blocks the binding of fibrinogen to platelets produces a thrombasthenic-like state in normal platelets and binds to glycoproteins IIb and/or IIIa. *J. Clin. Invest.* **72,** 325–338 (1983).
20. Kamata, T., Tieu, K. K., Springer, T. A. & Takada, Y. Amino acid residues in the αIIb subunit that are critical for ligand binding to integrin αIIbβ3 are clustered in the β-propeller model. *J. Biol. Chem.* **276,** 44275–44283 (2001).
21. Artoni, A. *et al.* The specificity determining loop and α helix 1 on human integrin β3 determine the binding of murine monoclonal antigbody 7E3 to αIIbβ3: implications for the mechanism of integrin activation. *Proc. Natl Acad. Sci. USA* (in the press) (2004).
22. Zavortink, M., Bunch, T. A. & Brower, D. L. Functional properties of alternatively spliced forms of the *Drosphila* PS2 integrin α subunit. *Cell Adhes. Commun.* **1,** 251–264 (1993).
23. von der Mark, H. *et al.* Alternative splice variants of α7β1 integrin selectivity recognize different laminin isoforms. *J. Biol. Chem.* **277,** 6012–6016 (2002).
24. Springer, T. A. Predicted and experimental structures of integrins and β-propellers. *Curr. Opin. Struct. Biol.* **12,** 802–813 (2002).
25. Lee, J.-O., Rieu, P., Arnaout, M. A. & Liddington, R. Crystal structure of the A domain from the α subunit of integrin CR3 (CD11b/CD18). *Cell* **80,** 631–638 (1995).
26. Lee, J.-O., Bankston, L. A., Arnaout, M. A. & Liddington, R. C. Two conformations of the integrin A-domain (I-domain): a pathway for activation? *Structure* **3,** 1333–1340 (1995).
27. Shimaoka, M. *et al.* Structures of the αL I domain and its complex with ICAM-1 reveal a shape-shifting pathway for integrin regulation. *Cell* **112,** 99–111 (2003).
28. Scarborough, R. M. & Gretler, D. D. Platelet glycoprotein IIb-IIIa antagonists as prototypical integrin blockers: novel parenteral and potential oral antithrombotic agents. *J. Med. Chem.* **43,** 3453–3473 (2000).
29. Gottschalk, K. E. & Kessler, H. The structures of integrins and integrin-ligand complexes: implications for drug design and signal transduction. *Angew. Chem. Int. Edn Engl.* **41,** 3767–3774 (2002).
30. Egbertson, M. S. *et al.* Non-peptide GPIIb/IIIa inhibitors. 20. Centrally constrained thienothiophene alpha-sulfonamides are potent, long acting *in vivo* inhibitors of platelet aggregation. *J. Med. Chem.* **42,** 2409–2421 (1999).
31. Scarborough, R. M. *et al.* Design of potent and specific integrin antagonists. *J. Biol. Chem.* **268,** 1066–1073 (1993).
32. Mould, A. P. *et al.* Integrin activation involves a conformational change in the α1 helix of the β subunit A-domain. *J. Biol. Chem.* **277,** 19800–19805 (2002).
33. Chen, J. F., Salas, A. & Springer, T. A. Bistable regulation of integrin adhesiveness by a bipolar metal ion cluster. *Nature Struct. Biol.* **10,** 995–1001 (2003).
34. Perutz, M. F. Mechanisms of cooperativity and allosteric regulation in proteins. *Q. Rev. Biophys.* **22,** 139–237 (1989).
35. Love, C. A. *et al.* The ligand-binding face of the semaphorins revealed by the high-resolution crystal structure of SEMA4D. *Nature Struct. Biol.* **10,** 843–848 (2003).
36. Bork, P., Doerks, T., Springer, T. A. & Snel, B. Domains in plexins: Links to integrins and transcription factors. *Trends Biochem. Sci.* **24,** 261–263 (1999).
37. Calvete, J. J., Henschen, A. & González-Rodríguez, J. Assignment of disulphide bonds in human platelet GPIIIa. A disulphide pattern for the β-subunits of the integrin family. *Biochem. J.* **274,** 63–71 (1991).
38. Beglova, N., Blacklow, S. C., Takagi, J. & Springer, T. A. Cysteine-rich module structure reveals a fulcrum for integrin rearrangement upon activation. *Nature Struct. Biol.* **9,** 282–287 (2002).
39. Newman, P. J., Derbes, R. S. & Aster, R. H. The human platelet alloantigens, PlA1 and PlA2, are associated with a leucine33/proline33 amino acid polymorphism in membrane glycoprotein IIIa, and are distinguishable by DNA typing. *J. Clin. Invest.* **83,** 1778–1781 (1989).
40. Watkins, N. A. *et al.* HPA-1a phenotype-genotype discrepancy reveals a naturally occurring Arg93Gln substitution in the platelet β3 integrin that disrupts the HPA-1a epitope. *Blood* **99,** 1833–1839 (2002).
41. Kunicki, T. J. *et al.* The P1A alloantigen system is a sensitive indicator of the structural integrity of the amino-terminal domain of the human integrin β3 subunit. *Blood Cells Mol. Dis.* **21,** 131–141 (1995).
42. Chen, J. F. *et al.* The relative influence of metal ion binding sites in the I-like domain and the interface with the hybrid domain on rolling and firm adhesion by integrin α4β7. *J. Biol. Chem.* (in the press).
43. Luo, B.-H., Takagi, J. & Springer, T. A. Locking the β3 integrin I-like domain into high and low affinity conformations with disulfides. *J. Biol. Chem.* **279,** 10215–10221 (2004).
44. Yang, W., Shimaoka, M., Chen, J. F. & Springer, T. A. Activation of integrin β subunit I-like domains by one-turn C-terminal α-helix deletions. *Proc. Natl Acad. Sci. USA* **101,** 2333–2338 (2004).
45. Takagi, J., Erickson, H. P. & Springer, T. A. C-terminal opening mimics "inside-out" activation of integrin α5β1. *Nature Struct. Biol.* **8,** 412–416 (2001).
46. Esnouf, R. M. An extensively modified version of MolScript that includes greatly enhanced coloring capabilities. *J. Mol. Graph. Model.* **15,** 132–138 (1997).
47. Merritt, E. A. & Murphy, M. E. P. Raster 3D version 2.0: a program for photorealistic graphics. *Acta Crystallogr. D* **50,** 869–873 (1994).
48. Carson, M. Ribbons. *Methods Enzymol.* **277,** 493–505 (1997).
49. Puzon-McLaughlin, W., Kamata, T. & Takada, Y. Multiple discontinuous ligand-mimetic antibody binding sites define a ligand binding pocket in integrin αIIbβ3. *J. Biol. Chem.* **275,** 7795–7802 (2000).
50. Tozer, E. C., Liddington, R. C., Sutcliffe, M. J., Smeeton, A. H. & Loftus, J. C. Ligand binding to integrin $\alpha_{IIb}\beta3$ is dependent on a MIDAS-like domain in the β3 subunit. *J. Biol. Chem.* **271,** 21978–21984 (1996).

Supplementary Information accompanies the paper on **www.nature.com/nature**.

Acknowledgements We thank colleagues in the Springer laboratory for supporting data and stimulating discussions, B. Kessler for tandem mass spectrometry, E. Yvonne Jones at Oxford for sema4D coordinates, members of the J.H.W. and M. Eck laboratories and the staff at APS and CHESS for assistance with crystallography, M. Gerstein and N. Echols (Yale University) for the morphing script used in producing movies, and Y. Cheng for help with comparing crystal structures and the electron microscopy map. Supported by NIH grants to T.A.S., J.H.W. and B.S.C.

Competing interests statement The authors declare competing financial interests: details accompany the paper on **www.nature.com/nature**.

Correspondence and requests for materials should be addressed to T.A.S. (springer@cbr.med.harvard.edu). Atomic coordinates and structural factors have been deposited with the Protein Data Bank with the accession codes 1TY3 (form A + cacodylate 1); 1TXV (form A + cacodylate 2); 1TY5 (form A + tirofiban); 1TY6 (form A + eptifibatide); 1TY7 (form A + L-739758); 1TYE (form B + cacodylate). Sequences of the 10E5 Fab have been deposited with GenBank.

Supplementary material

Results

The cap subdomain and binding of 10E5 Fab

The cap subdomain of α_{IIb} comprises four insertions in the β-propeller, which include two β hairpins (β-A/β-B and β-C/β-D) in inserts 1 and 2 that form a four-stranded antiparallel β sheet, and two α helices (α-A and α-B) in inserts 3 and 4 (Supplementary Fig. 1A and 2). The first β hairpin is inserted in the 4-1 loop between β-propeller blades 1 and 2, and the second in the loop between β-strands 2 and 3 of blade 2. The α-A helix is in the 4-1 loop between blades 2 and 3, and the α-B helix plus a long loop are inserted between β-strands 3 and 4 of blade 3. Inserts 1-3 emanate from loops on the "upper" face of the propeller, whereas insert 4 emanates from a "bottom" loop.

The cap is an elaboration of the β-propeller that is specialized as a ligand binding surface, correlating with marked variation in length and sequence of the inserts among α subunits. Although composed of four inserts and hence not modular like the I domain, the cap subdomain has a similar although not exclusive role in ligand binding. There is no evidence that cap loops change conformation in response to conformational change in the β I-like domain, although such a specialization could have been a precursor to the evolution of I domain-containing integrins.

The major residues contributed by the cap subdomain to the interface with 10E5 are in the β-turn in the β-A/β-B hairpin (residues Arg77 to Gln82), and the long loop after α-B (residues Ser206, Arg208, Leu213, Trp214 and His215) (Supplementary Fig. 2). The α-A helix contributes two hydrogen bonds by residues Asn149 and Asn158. On the 10E5 side of the interface, all six of its complementarity determining region loops participate in binding, and contribute eight tyrosines that dominate the interface. A total of 1770 $Å^2$ solvent accessible surface area is buried at the interface, typical of antibody-antigen complexes [1].

The functional importance of the cap domain in ligand binding is supported by the localization of the 10E5 epitope to the cap domain since 10E5 effectively inhibits ligand binding [2]. Further support comes from studies in which mutations in the cap domain decreased ligand binding (Fig. 2f) [3]. The binding of 10E5 exclusively to the cap domain also explains 10E5's specificity for $\alpha_{IIb}\beta_3$ since the cap domain amino acids that interact with 10E5 are not conserved in $\alpha_v\beta_3$ (Supplementary Figs. 1A and 2) [4].

Although the cap interacts with 10E5 in crystal form A, the interaction with 10E5 did not significantly affect the cap structure as judged by the cap structure being essentially the same in the three independent heterodimers in crystal form B prepared in the absence of 10E5 Fab (Fig. 1b). 10E5 prevents dissociation of the α_{IIb} and β_3 subunits on platelets in the presence of EDTA and high pH and temperature [4]. We noted that 10E5 prevents α_{IIb} and β_3 dissociation in size-exclusion chromatography, and that the $\alpha_{IIb}\beta_3$:10E5 complex is more resistant to protease digestion than uncomplexed $\alpha_{IIb}\beta_3$. Like divalent cations, 10E5 stabilizes the $\alpha_{IIb}\beta_3$ headpiece complex without binding across an α_{IIb} interface with β_3. Hence, 10E5 stabilizes the native fold of α_{IIb}, and since native α_{IIb} and not disordered α_{IIb} binds to β_3, also the $\alpha_{IIb}\beta_3$ complex.

Drug binding

Integrin $\alpha_{IIb}\beta_3$ binds to physiologic ligands containing Arg-Gly-Asp sequences and to a similar Lys-Gln-Ala-Gly-Asp-Val sequence in fibrinogen [5]. Each co-crystallized ligand-mimetic possesses a basic group (the Lys mimetic) that hydrogen bonds to the requisite Asp-224 residue [3] in a cleft of the α_{IIb} β-propeller, and a carboxylate (the Asp mimetic) that extends in the opposite direction and coordinates the Mg^{2+} of the MIDAS of the β_3 I-like domain (Fig. 2a-c). Several loops make prominent projections that form a wall around the drug-binding pocket at the α_{IIb} interface with β_3. In the α_{IIb} β-propeller, the 4-1 loops connecting blades 2 and 3 (residues 147-166) and connecting blades 3 and 4 (residues 224-234) form walls on either side of the Lys mimetic. The first of these loops

contains α-helix residues including Phe-160 that contact the aliphatic portion of the Lys mimetic (Fig. 2a-c), and are essential for fibrinogen binding [3]. The long insertion containing this α-helix corresponds to cap subdomain insert 3 (see below), and corresponds in insertion position to where the I domain is inserted in integrins that contain I domains. Phe-231 in the blade 3 to blade 4 loop is prominent in the wall on the other side of the aliphatic amine pocket, while Tyr-190 in the loop between β-strands 2 and 3 of blade 2 of the propeller forms the floor of the pocket. Both aromatic residues are indispensable for fibrinogen binding [3]. At the opposite, carboxyl end of the drug molecules, the β1-α1 loop of the β_3 I-like domain forms another wall of the pocket. This loop contains an Asp-Leu-Ser-Tyr-Ser-Met-Lys-Asp-Asp sequence in which all Asp and Ser residues coordinate the MIDAS or ADMIDAS metal ions, and Tyr122 lines the wall. Nearby Arg214 also lines the pocket. Both Tyr122 and Arg214 are implicated in fibrinogen binding [6 7] and/or etiology of Glanzmann thrombasthenia [8]. These residues also donate backbone hydrogen bonds to the non-metal coordinating oxygen of the drug carboxylate group (Fig. 2a-e).

Eptifibatide (Fig. 2b) was developed as a cyclic heptapeptide mimic of barbourin, a snake venom disintegrin [5]. A Lys-Gly-Asp-Trp sequence in barbourin, incorporated in eptifibatide except for guanidation of the Lys to convert it to homoarginine, renders both antagonists highly selective for $\alpha_{IIb}\beta_3$ [9]. By contrast, disintegrins and peptides with RGD sequences also bind to $\alpha_V\beta_3$. The structures reveal the basis for this specificity. The aliphatic moieties of Lys, and its homoarginine derivative in eptifibatide, are one methylene longer than that of Arg. In the blade 3 to blade 4 loop of the α_{IIb} β-propeller, Phe231 replaces Arg218 of α_V, in a favorable position to make hydrophobic contacts with the aliphatic portion of Lys or homoarginine sidechains, but not the shorter aliphatic moiety in Arg (Fig. 2b, d). Furthermore, a single Asp224 residue in α_{IIb} instead of the two Asp150 and Asp218 residues in α_V is available for hydrogen bonding, and it is more deeply buried, thus requiring a longer sidechain to reach it (Fig. 2b, d). Studies with

cyclic Arg-Gly-Asp peptides suggested that longer and shorter distances between Arg Cα and Asp Cα atoms favor selectivity for $\alpha_{IIb}\beta_3$ and $\alpha_V\beta_3$, respectively [10]. Indeed, the hydrogen-bonding guanidinium moiety of eptifibatide bound to $\alpha_{IIb}\beta_3$ extends further than that of cyclo-RGDfV bound to $\alpha_V\beta_3$, as a result both of the extra methylene in the sidechain and a backbone flip between the Cα atoms of the basic and Gly residues (Fig. 2b, d). Furthermore, capping the basic moiety with an aromatic group greatly decreases binding to $\alpha_{IIb}\beta_3$ but not $\alpha_V\beta_3$, in agreement with hydrogen bonds that are end-on to α_{IIb} and side-on to α_V [10] (Fig. 2b, d).

Tirofiban and the high affinity Merck compound L-739758 are non-peptidomimetics [11]. They contain butyl or pyridyl sulfonamide substituents (Fig. 2a, c) that were found to substantially increase affinity and thus were postulated to bind to an "exosite." The co-crystal structures demonstrate that the butyl and pyridyl groups fold back over and are in intimate van der Waals contact with the linker between the drug amine and carboxyl groups, and essentially thicken the drugs. The butyl and pyridyl sulfonamide groups thus pick up interactions with both α_{IIb} and β_3 residues. The sulfonamide hydrogen bonds to β_3 residues Tyr166 and Arg214, and the butyl and pyridyl groups interact with α_{IIb} residues Phe160 and Tyr190. The Trp residue in epitifibatide and disintegrins as well as linear Arg-Gly-Asp-Trp peptides markedly raises affinity for integrins [9]. Remarkably, in eptifibatide this Trp occupies the same exosite pocket as the pyridyl group in L-739758 (Fig. 2b, c).

The increase in affinity in the series eptifibatide < tirofiban << L-739758 [5] is accompanied by a decrease in number of bonds about which rotation is allowed, and hence a decrease in loss of entropy upon drug binding. Furthermore, additional hydrogen bonds are added involving the sulfonamide group, between the piperidine moieties and the backbone carbonyl of α_{IIb}-Ser225 (Fig. 2a, c), and between the pyridyl exosite substituent of L-739758 and α_{IIb}-Tyr190 (Fig. 2c).

LIBS and other epitopes in integrin ectodomain tertiary rearrangements

The presence of the PSI domain in our structure, the arrangement of I-EGF2 and 3 domains [12] and the structure of most domains in bent $\alpha_V\beta_3$ [13] allows a model to be constructed of bent $\alpha_V\beta_3$ that suggests that the extreme bend in the β_3 subunit occurs between the I-EGF1 and 2 domains (Fig. 5a). The HPA-1 epitope, known to be accessible on resting $\alpha_{IIb}\beta_3$, is well exposed on the PSI domain in the bent model, as are constitutively expressed AP3 and drug (quinine)-dependent epitopes at the PSI-hybrid domain interface [14] (Supplementary Fig. 4). In contrast, the AP5 activation-dependent LIBS epitope which localizes to mouse-human differences at residues 1 and 2 is partially masked in the bent conformation by the α subunit calf-1 domain (Supplementary Fig. 4). Activation epitopes in β_2 I-EGF domains 2 and 3 have similarly been shown to be buried in the bent conformation [12].

Methods

Protein expression, purification and crystallization

Because the leg domains of the β_3 subunit are flexible [15], we expressed $\alpha_{IIb}\beta_3$ headpiece constructs in CHO Lec.3.2.8.1 cells to obtain ligand-binding fragments amenable for crystallization. The soluble $\alpha_{IIb}\beta_3$ headpiece encompassing residues 1-621 of α_{IIb} and residues 1-472 of β_3 was expressed in CHO Lec 3.2.8.1 cells with an ACID-BASE coiled-coil clasp at the C-termini, as described for soluble $\alpha_5\beta_1$ [16], except that a hexahistidine tag was fused to the C-terminus of β_3. The expressed protein was fractionated and concentrated by 0-60% ammonium sulfate precipitation and the pellet re-dissolved in a buffer containing 25 mM Tris HCl (pH 8.0) and 300 mM NaCl, plus 1 mM $CaCl_2$ and 1 mM $MgCl_2$ (loading buffer). The solution was loaded onto a Ni-NTA matrix (QIAGEN) column (5 ml of resin per 1 liter of culture supernatant) pre-equilibrated in the above loading buffer. The column was then washed with ten bed-volumes of the loading buffer plus 20 mM imidazole and the bound proteins were eluted

with five bed-volumes of the loading buffer plus 250 mM imidazole. The washing and eluting steps were monitored by measuring the absorbance of the eluate at 280 nm. The eluted proteins were concentrated with 60% saturated ammonium sulfate, re-dissolved in 20 mM Tris HCl (pH 7.5) and 150 mM NaCl (TBS), plus 1 mM $CaCl_2$ and 1 mM $MgCl_2$, and subjected to size exclusion chromatography (Superdex 200 HR, Pharmacia) in the same buffer to remove aggregated species. The same buffer was also used for all following size exclusion chromatography steps. Such purified $\alpha_{IIb}\beta_3$ was concentrated with a Centriprep YM-30 centrifugal filter unit (Millipore, Billerica, MA) to about 1 mg/ml and treated with sequencing grade chymotrypsin (Roche) (10 μg enzyme per mg $\alpha_{IIb}\beta_3$) at 25°C for 16 hr in the TBS plus calcium and magnesium buffer. The digestion was stopped with 0.5 mM phenylmethylsulfonylfluoride and the unclasped (coiled-coil and His_6 tag removed) $\alpha_{IIb}\beta_3$ protein was collected in the flow-through of a second Ni-NTA chromatography step. Such purified $\alpha_{IIb}\beta_3$ was mixed with the 10E5 Fab (1:1.1 molar ratio) and the complex was purified by Superdex 200 chromatography. The purified complex was very stable and no dissociation of the α_{IIb} and β_3 subunits was detected in further chromatography steps. The complex was subjected to digestion with carboxypeptidase A and B (Calbiochem) (1:100 weight ratio) in the presence of 1 mM $ZnCl_2$ at 25°C for 16 hr. A stable protease resistant core of $\alpha_{IIb}\beta_3$ was obtained and further purified by a final Superdex 200 chromatography step and stored at 4°C in TBS plus calcium and magnesium, and used to obtain crystal form A. The migration pattern of the resulting sample on SDS-PAGE suggested that the thigh domain, which contains a chymotrypsin cleavage site, was removed by carboxypeptidase treatment. This was confirmed by tryptic digestion and tandem mass spectrometry of the SDS-PAGE bands of $\alpha_{IIb}\beta_3$ followed by a database search using the Mascot server (http://mascot.chip.org) (data not shown).

The human fibrinogen γ chain C-terminal fragment (residues 144-411) was expressed with HEK 293T cells as a fusion protein, with an N-terminal human growth

hormone domain, using the pSGHV0 vector (a gift from Dr. D.J. Leahy) [17]. The linker between the hGH sequence (…SCGF) and γ chain sequence (ITGKD…) was SGHHHHHHHHDYDSSENLYFQGS and contained a His_8 tag and TEV cleavage site. The fusion protein was purified by Ni-NTA chromatography with the same procedure as above for $\alpha_{IIb}\beta_3$, except the calcium and magnesium were omitted in all steps. This was followed by TEV cleavage (250 U/ml enzyme concentration, room temperature for 16 hr) in the loading buffer and a second Ni-NTA chromatography to remove the tag and the growth hormone. The $\alpha_{IIb}\beta_3$ fragment purified through the second Ni-NTA chromatography step was mixed with an excess of the purified fibrinogen fragment in the presence of 1mM $MnCl_2$ and subjected to carboxypeptidase A and B treatment. As shown by SDS-PAGE, this resulted in the same pattern of $\alpha_{IIb}\beta_3$ digestion as for the 10E5 complexed sample; however, little of the fibrinogen domain copurified with $\alpha_{IIb}\beta_3$ headpiece upon Superdex 200 chromatography, probably due to the hydrolysis of the $\alpha_{IIb}\beta_3$-binding C-terminal residues of the fibrinogen γ chain by carboxypeptidase. This material was used to obtain crystal form B, which contains no fibrinogen fragment.

The Topaz crystallizer from Fluidigm Corporation was utilized to identify initial crystallization conditions. Protein solution (3 μl) was screened at three different protein:reagent ratios against 48 different reagents from Hampton Research, Inc using free interface diffusion [18]. The lead conditions found were then optimized with hanging drop vapor diffusion in which an equal volume of protein solution (~10 mg/ml) was mixed with an equal volume of well solution on a siliconized glass coverslide and equilibrated against one milliliter of the well solution. The final optimized well solution for form A crystals of the 10E5 Fab: $\alpha_{IIb}\beta_3$ complex is 11% PEG 3350, 0.7 M magnesium acetate, and 0.1 M sodium cacodylate, pH 6.5, and for crystal form B is 10% PEG 8000, 0.4 M magnesium acetate and 0.1 M sodium cacodylate, pH 7.0. Acetate and 4°C temperature were absolutely required for crystallization. Crystal form A was harvested in the mother liquor, supplemented with glycerol as a cryoprotectant in 5% increments up to

a 20% final concentration, and then flash frozen in liquid nitrogen. Crystal form B was much more fragile than form A and could only be stabilized in the mother liquor with increasing concentrations of magnesium acetate to 1.36 M as cryoprotectant. Before co-crystals of the 10E5/$\alpha_{IIb}\beta_3$ complex with drugs were obtained, native crystals (form A) were soaked for up to 16 hours with drugs. One of the tirofiban-soaked crystals diffracted better (2.7 Å) than the native crystals (native1, 2.8 Å). Diffraction data from such crystals showed that the MIDAS was still occupied by cacodylate buffer ion instead of drug, which was verified by a large anomalous difference Fourier peak from the cacodylate arsenic atom near the MIDAS, a feature found in the native but not drug co-crystals (see below). Comparison of the structures from the soaked and native crystals suggested that the structures were essentially the same. Therefore, the 2.7 Å resolution structure is regarded as the native structure (native2). From then on, co-crystallization with drugs was in the presence of positively charged imidazole buffer ions instead of the negatively charged cacodylate buffer. Specifically, the protein sample was mixed with each drug at 1:3 to 1:5 molar ratios before setting up the hanging drops, and the optimized well solutions were 10-12% PEG 3350, 0.7 M magnesium acetate, and 0.1 M imidazole (pH 6.5) for the co-crystals. Crystals were flash frozen in a manner similar to that of the native crystals, except that drugs were supplemented in all of the cryo-solutions.

Compound L-739758 was the kind gift of Dr. G. Hartman, Merck Research Laboratories, West Point, NY. Tirofiban and eptifibatide were from Merck (Whitehouse Station, NJ) and Millennium Pharmaceuticals (South San Francisco, CA), respectively. 10E5 Fab was prepared using immobilized papain (Pierce, Rockford, IL) and Protein A affinity chromatography according to the manufacturer's instructions.

Data collection and structural determination

Diffraction data were collected at the 19-ID station of the Advanced Photon Source (APS) at the Argonne National Laboratory and the A-1 station of the Cornell High Energy Synchrotron Source (CHESS), and processed with program suite HKL2000 [19]. For crystal form A, analysis of the diffraction data suggested a primitive hexagonal crystal system. The program AMoRe [20] was used for molecular replacement. The hexagonal spacegroups were tested with several models including the β-propeller and/or I-like domains from $\alpha_V\beta_3$ (PDB ID 1L5G), and different antibody Fab structures from the protein data bank. One clear molecular replacement solution each was obtained when space group $P3_221$ was tested with search models of the I-like domain and the I-like domain plus the β-propeller from $\alpha_V\beta_3$, and a murine Fab 36-71 (PDB ID 6FAB). Visual inspection of the molecular replacement solutions using program O [21] indicated good molecular packing in the unit cell of the independently obtained solutions from different search models. Electron density maps calculated using phases from the search models clearly showed the presence of the hybrid domain, plus difference densities in the CDR loops of the Fab. The structure of crystal form B was solved by molecular replacement using the $\alpha_{IIb}\beta_3$ structure in crystal form A as a search model. No fibrinogen γ chain fragment was present in the electron density map.

The solutions from molecular replacement were subjected to iterative cycles of model rebuilding in O and refinement using CNS (version 1.1) protocols for rigid body refinement, positional refinement by Powell minimization, group or individual B factor refinement, and slow-cool simulated annealing molecular dynamics [22]. Anisotropic temperature factor correction, bulk solvent correction, and maximum likelihood refinement target were applied throughout. Sigma A weighted 2*Fo-Fc* and *Fo-Fc* maps were computed for visual inspection during rebuilding of the model and the refinement was monitored by the decrease of the R_{free}.

In the β_3 I-like domain, the presence of a calcium ion at the ADMIDAS but not MIDAS is validated by the presence and absence, respectively of a strong anomalous

difference Fourier peak calculated using data from an ytterbium-soaked crystal prepared by soaking the crystals overnight in a cryosolution that contains 10 mM $YbCl_3$ and no calcium or magnesium. Deep burial of the LIMBS metal binding site may have prevented fast exchange of the bound metal with heavy metals such as ytterbium. Nonetheless, the rich presence of backbone carbonyl groups in the LIMBS coordination sphere is compatible with Ca^{2+} and not Mg^{2+} [23,24]. Similarly strong anomalous difference Fourier peaks were found in the ytterbium-soaked crystals at the β hairpin Ca^{2+}-binding motifs [25] in β-propeller blades 4, 6, and 7; Ca^{2+} was also assigned at the more deeply buried β hairpin Ca^{2+}-binding motif in blade 5.

The first loop of the hybrid domain (residues Ser70-Val80) is exposed to the solvent in the crystal lattice and has poor electron density, suggesting multiple conformations. However, there is clear continuous density connecting the mainchain of the two β strands N- and C-terminal to this loop and excellent densities for some of the landmark residues (i.e., Phe56, Pro57, Pro68 and Leu69). This allowed unambiguous anchoring of the loop. After cycles of manual rebuilding and simulated annealing refinement, the resulting model for the loop may represent one of the most stable conformers.

The structure of the PSI domain was built based on the electron density maps computed with the refined models and guided by the secondary structure arrangements in the sema4D crystal structure [26]. The conserved disulfides and the single tryptophan in the domain also facilitated tracing (Supplementary Fig. 3). There are very good electron densities for all of the disulfides and the α3 helix, and good densities for the rest of the secondary structures, except for the α1 helix near residue Gly9. Continuous electron density extends beyond residue Cys435 and allowed the building of residues Ala436 to Gln440 in the structure. Residues 437-440 of I-EGF1 make intimate contacts with the PSI domain through multiple hydrogen bonds. It appears that most of I-EGF1 is either disordered or was removed by carboxypeptidase digestion, although density is evident for

a portion of the residue that disulfide-bonds to residue Cys437. Because of the hydrophilic nature of the interactions with residues 437-440 and the absence of electron density for the bulk of the I-EGF1 domain, we cannot rule out the possibility that this portion of I-EGF1 may contact the PSI domain in alternative manners.

In crystal form A, five N-linked glycan chains were built, one of which contains seven sugar rings, and is involved in crystal lattice contacts. The electron density for the glycan chains is weaker in crystal form B, partly because they are not in good crystal lattice contacts as in form A. Therefore, only 3 to 4 chains are built for individual heterodimers in form B. Water molecules were added to the models based on visual inspection of the peaks in the 2*Fo-Fc* maps calculated using the refined models. Waters with at least one hydrogen bond to protein atoms and a temperature factor below 80 $Å^2$ after refinement were included in the final models.

The structures of the drug bound $\alpha_{IIb}\beta_3$ were solved by molecular replacement using the native structure as a search model. Electron density for the bound drug molecules was readily discernible in the maps calculated with the molecular replacement solution. Topology and parameter files of the drugs were constructed using program XPLO2D (Uppsala Software Factory), the CORINA server (http://www2.chemie.uni-erlangen.de/software/corina/index.html) and PRODRG server (http://davapc1.bioch.dundee.ac.uk/programs/prodrg/). Model building and refinement were carried out essentially as above. Calculation of the hybrid domain swingout angle was performed with program HINGE by Peter Sun (http://red.niaid.nih.gov/programs/hinge.html). Other structural analysis was performed with the CCP4 program suite [27], CNS [22] and the Uppsala Software Factory [21] (http://alpha2.bmc.uu.se/~gerard/manuals/welcome2usf.html).

Hybrid domain sequence-to-structure register

Comparison to our hybrid domain structure suggests that previous β_3 structures are one residue out of sequence-structure register for residues 55 to 77. Our register is supported by the excellent electron density in our maps for the sidechains of Phe56, Pro57, Pro68, and Leu69 (Supplementary Fig. 3a). Residues in the adjacent PSI domain, which were disordered in previous structures, also provided landmarks for the chain trace. The region in question is anchored by a well-formed 6-residue β-strand, and by multiple nearby disulfide bonds in the hybrid and PSI domains (Fig. 5f).

Superposition

For comparison between β_3 I-like domains, superposition was with residues 112-119, 149-157, 189-196, 243-250, 303-309, and 328-332, (Fig. 3c); essentially equivalent superpositions shown in figures were with β-sheet residues.

Determination of the 10E5 Fab sequence

Total RNA was extracted from 10E5 hybridoma cells [2] with the RNeasy RNA extraction kit (QIAGEN, Valencia, CA). The cDNA encoding the 10E5 Fab fragment was obtained by reverse transcription and PCR amplification using OneStep RT-PCR kit from QIAGEN and cloned into the pDrive vector (QIAGEN). Sequences for the RT-PCR primers were obtained from Novagen (Madison, WI) mouse Ig-Primer Sets Technical Bulletin TB326 and references therein. Primers were synthesized by IDT, Inc (Coralville, CA). DNA sequencing was performed by SeqWright, Inc (Houston, TX).

Supplementary Figure 1. Sequence alignment of the portions of α and β subunits structurally defined here. A. The α-subunit β-propeller domain and cap subdomain. The α_{IIb} and α_V sequences are aligned structurally and other representative integrin α subunits are aligned by sequence. The β strands from the seven blades of α_{IIb} and α_V are marked in magenta letters and underlines. Positions of the four cap inserts are shown with

arrows. The inserted β strands and α helices in α_{IIb} are underlined and marked green and blue, respectively. The positions of the I domains for α_L and α_2 are indicated by a red arrow. The fibrinogen binding-sensitive residues are highlighted in yellow. Every tenth residues of α_{IIb} is marked with a dot above the residue. Disulfides are denoted with an orange line connecting the cysteines. The four calcium-binding sites are marked with cyan lines. B. Sequence alignment of the PSI, hybrid, and I-like domains of representative integrins. Color coding is similar to A. Secondary structures for liganded-open $\alpha_{IIb}\beta_3$ and unliganded-closed $\alpha_V\beta_3$ are shown as lines above and below the sequence, respectively. α-helix and 3_{10}-helix are shown as blue and green lines, respectively. Residues with sidechains that coordinate metal ions are colored, and those with metal-coordinating backbone carbonyls are asterisked below the alignment. Letters and asterisks are red (MIDAS), green (ADMIDAS), and blue (LIMBS).

Supplementary Figure 2. Stereo-view of the $\alpha_{IIb}\beta_3$:10E5 interface. The β-propeller, light and heavy chains of 10E5 are shown as magenta, cyan and blue ribbons, respectively. The interface residues are shown as ball-and-stick models and the hydrogen bonds as dotted lines. The secondary structures in the β-propeller are labeled.

Supplementary Figure 3. Representative electron density in the hybrid and PSI domains. Electron density (2*Fo-Fc*) maps contoured at 1 σ are shown for the βX and βA' strands of the hybrid domain (A) and the PSI domain (B). The disulfide bonds and the conserved Trp25 are marked in B.

Supplementary Figure 4. Mapping of the epitopes for the inhibitory and activating antibodies on open and closed integrin structures. Epitopes for $\alpha_{IIb}\beta_3$ and homologous residues for epitopes from β_1 and β_2 integrins are shown. See references [3] [28] references therein, and [29,30]. The open $\alpha_{IIb}\beta_3$ headpiece structure (**a**) and closed, bent $\alpha_V\beta_3$ structure

[13] with our PSI domain structure added (**b-d**) are shown. The α and β subunits are shown in silver and gold, respectively, except the β PSI domain is green. The orientation of the β-propeller and I-like domains in **a** and **b** are identical. The view in **c** is rotated 90 degrees along the vertical axis from the view in **b**, and the view in **d** is rotated about 140 degrees along an axis perpendicular to the plane of the paper from the view in **c**. The epitopes for inhibitory, activating and both types of monoclonal antibodies are shown as cyan, magenta and black spheres, respectively. The HPA-1 allo-antigen epitope [31] and drug-dependent epitopes [14] are shown as gold and green spheres, respectively. The epitope for anti-LIBS antibody AP5 is marked with dotted circles.

Supplementary movie 1. Allostery in the integrin headpiece. The transition from the unliganded, closed headpiece [13] to the liganded, open headpiece is shown by adding the PSI domain to the closed structure and creating interpolated images of the β_3 subunit with program Pymol by W.L. DeLano (http://www.pymol.org).

Supplementary Table 1. Statistics of X-ray diffraction data collection and structure refinement

Crystal form A	Native1	Native2	Tirofiban	Eptifibatide	L-739758	**Crystal form B**
Spacegroup	$P3_221$	$P3_221$	$P3_221$	$P3_221$	$P3_221$	$P6_2$
Unit cell (a, b, c) (Å)	148.9,148.9,176.1	148.9,148.9,176.4	148.6,148.6,177.2	149.6,149.6,175.7	149.2,149.2,176.2	332.1,332.1, 88.3
(α, β, γ) (°)	90,90,120	90,90,120	90,90,120	90,90,120	90,90,120	90,90,120
Wavelength (Å)	0.9793	0.9793	0.9760	0.9760	0.9793	0.9760
Resolution (Å)	50-2.8	50-2.7	50-2.9	50-2.9	50-3.1	50-2.9
Number of reflections	400,460/	442,121/	330,745/	357,439/	263,308/	1,251,268/
(total/unique)	55,875	62,512	50,662	50,647	41,586	122,126
Completeness (%)	99.9/99.8*	99.9/100*	99.7/98.2*	100/100*	99.8/99.7*	98.2/93.9*
I/σ(I)	14.0/3.1*	20.0/3.0*	12.1/2.0*	14.9/2.7*	12.1/2.7*	17.4/3.0*
Rmerge (%)[¶]	13.0/68.1*	9.6/59.8*	13.9/57.8*	11.7/61.5*	14.0/55.8*	9.7/60.2*
Number of protein/	10165/653	10165/655	10165/419	10165/574	10165/254	20604/415
hetero-atoms						
Rmsd bond lengths	0.008 Å	0.007 Å	0.008 Å	0.008 Å	0.009 Å	0.011 Å
Rmsd bond angles	1.5°	1.6°	1.5°	1.5°	1.5°	1.7°
Rwork[¶¶]	20.6 %	20.1 %	21.1 %	20.0 %	22.6 %	21.9 %
Rfree[‡‡]	23.6 %	24.2 %	24.5 %	23.4 %	27.0 %	25.4 %
Ramachandran plot**	80.6%/17.6%/	82.3%/16.7%/	80.1%/18.3%/	81.5%/17.2%/	78.8%/19.2%/	80.5%/18.6%/
	1.8%/0%	1.0%/0%	1.6%/0%	1.3%/0%	2.0%/0%	0.9%/0%
PDB code	1TY3	1TXV	1TY5	1TY6	1TY7	1TYE

*Asterisked numbers correspond to the last resolution shell.

¶ $R_{merge} = \Sigma_h \Sigma_i |I_i(h) - \langle I(h) \rangle| / \Sigma_h \Sigma_i I_i(h)$, where $I_i(h)$ and $\langle I(h) \rangle$ are the ith and mean measurement of the intensity of reflection *h*.

¶¶ $R_{work} = \Sigma_h ||F_{obs}(h)| - |F_{calc}(h)|| / \Sigma_h |F_{obs}(h)|$, where $F_{obs}(h)$ and $F_{calc}(h)$ are the observed and calculated structure factors, respectively. No I/σ cutoff was applied.

‡‡ R_{free} is the R value obtained for a test set of reflections consisting of a randomly selected 5% subset of the data set excluded from refinement.

** Residues in core (most favorable), allowed, additional allowed, and disallowed regions of the Ramachandran plot as reported by Procheck [32].

References.

1. Janin, J. & Chothia, C. The structure of protein-protein recognition sites. *J. Biol. Chem.* **265**, 16027-16030 (1990).

2. Coller, B. S., Peerschke, E. I., Scudder, L. E. & Sullivan, C. A. A murine monoclonal antibody that completely blocks the binding of fibrinogen to platelets produces a thrombasthenic-like state in normal platelets and binds to glycoproteins IIb and/or IIIa. *J. Clin. Invest.* **72**, 325-338 (1983).

3. Kamata, T., Tieu, K. K., Springer, T. A. & Takada, Y. Amino acid residues in the αIIb subunit that are critical for ligand binding to integrin αIIbβ3 are clustered in the β- propeller model. *J. Biol. Chem.* **276**, 44275-44283 (2001).

4. Coller, B. S. et al. Studies on the binding of an alloimmune and two murine monoclonal antibodies to the platelet glycoprotein IIb-IIIa complex receptor. *J. Lab. Clin. Med.* **107**, 384-392 (1986).

5. Scarborough, R. M. & Gretler, D. D. Platelet glycoprotein IIb-IIIa antagonists as prototypical integrin blockers: novel parenteral and potential oral antithrombotic agents. *J. Med. Chem.* **43**, 3453-3473 (2000).

6. D'Souza, S. E. et al. Ligand and cation binding are dual functions of a discrete segment of the integrin β_3 subunit: Cation displacement is involved in ligand binding. *Cell* **79**, 659-667 (1994).

7. Charo, I. F., Nannizzi, L., Phillips, D. R., Hsu, M. A. & Scarborough, R. M. Inhibition of fibrinogen binding to GP IIb-IIIa by a GP IIIa peptide. *J. Biol. Chem.* **266**, 1415-1421 (1991).

8. French, D. L. & Coller, B. S. Hematologically important mutations: Glanzmann thrombasthenia. *Blood Cells, Mol.Dis.* **23**, 39-51 (1997).

9. Scarborough, R. M. et al. Design of potent and specific integrin antagonists. *J. Biol. Chem.* **268**, 1066-1073 (1993).

10. Gottschalk, K. E. & Kessler, H. The structures of integrins and integrin-ligand complexes: implications for drug design and signal transduction. *Angew. Chem. Int. Ed. Engl.* **41**, 3767-3774 (2002).

11. Egbertson, M. S. et al. Non-peptide GPIIb/IIIa inhibitors. 20. Centrally constrained thienothiophene alpha-sulfonamides are potent, long acting in vivo inhibitors of platelet aggregation. *J. Med. Chem.* **42**, 2409-2421 (1999).

12. Beglova, N., Blacklow, S. C., Takagi, J. & Springer, T. A. Cysteine-rich module structure reveals a fulcrum for integrin rearrangement upon activation. *Nat. Struct. Biol.* **9**, 282-287 (2002).

13. Xiong, J.-P. et al. Crystal structure of the extracellular segment of integrin αVβ3. *Science* **294**, 339-345 (2001).

14. Peterson, J. A., Nyree, C. E., Newman, P. J. & Aster, R. H. A site involving the "hybrid" and PSI homology domains of GPIIIa (β3-integrin subunit) is a common target for antibodies associated with quinine-induced immune thrombocytopenia. *Blood* **101**, 937-942 (2003).

15. Takagi, J., Petre, B. M., Walz, T. & Springer, T. A. Global conformational rearrangements in integrin extracellular domains in outside-in and inside-out signaling. *Cell* **110**, 599-611 (2002).

16. Takagi, J., Erickson, H. P. & Springer, T. A. C-terminal opening mimics "inside-out" activation of integrin α5β1. *Nature Struct. Biol.* **8**, 412-416 (2001).

17. Leahy, D. J., Dann, C. E., Longo, P., Perman, B. & Ramyar, K. X. A mammalian expression vector for expression and purification of secreted proteins for structural studies. *Protein Expr. Purif.* **20**, 500-506. (2000).

18. Hansen, C. L., Skordalakes, E., Berger, J. M. & Quake, S. R. A robust and scalable microfluidic metering method that allows protein crystal growth by free interface diffusion. *Proc. Natl. Acad. Sci. U S A* **99**, 16531-16536 (2002).

19. Otwinowski, Z. & Minor, W. Processing of X-ray diffraction data collected in oscillation mode. *Methods in Enzymology* **276**, 307-326 (1997).

20. Navaza, J. Amore: An automated package for molecular replacement. *Acta Crystallographica* **A50**, 157-163 (1994).

21. Jones, T. A. & Kjeldgaard, M. (ed. Uppsala) 1-161 (Uppsala University, 1993).

22. Brunger, A. T. et al. Crystallography & NMR System: a new software suite for macromolecular structure determination. *Acta Crystallgr. D.* **54**, 905-921 (1998).

23. Harding, M. M. The architecture of metal coordination groups in proteins. *Acta Crystallogr. D Biol. Crystallogr.* **60**, 849-859 (2004).

24. Chen, J. F., Salas, A. & Springer, T. A. Bistable regulation of integrin adhesiveness by a bipolar metal ion cluster. *Nat. Struct. Biol.* **10**, 995-1001 (2003).

25. Springer, T. A. Predicted and experimental structures of integrins and β-propellers. *Curr. Opin. Struct. Biol.* **12**, 802-813 (2002).

26. Love, C. A. et al. The ligand-binding face of the semaphorins revealed by the high-resolution crystal structure of SEMA4D. *Nat. Struct. Biol.* **10**, 843-848 (2003).

27. Bailey, S. The CCP4 suite-programs for protein crystallography. *Acta Crystallogr. D Biol. Crystallogr.* **50**, 760-763 (1994).

28. Humphries, M. J., Symonds, E. J. & Mould, A. P. Mapping functional residues onto integrin crystal structures. *Curr. Opin. Struct. Biol.* **13**, 236-243 (2003).

29. Luo, B.-H., Strokovich, K., Walz, T., Springer, T. A. & Takagi, J. Allosteric β1 integrin antibodies that stabilize the low affinity state by preventing the swing-out of the hybrid domain. *J. Biol. Chem.* **279**, 27466-27471 (2004).

30. Mould, A. P. et al. Conformational changes in the integrin βA domain provide a mechanism for signal transduction via hybrid domain movement. *J. Biol. Chem.* **278**, 17028-17035 (2003).

31. Newman, P. J., Derbes, R. S. & Aster, R. H. The human platelet alloantigens, PlA1 and PlA2, are associated with a leucine33/proline33 amino acid polymorphism in membrane glycoprotein IIIa, and are distinguishable by DNA typing. *J. Clin. Invest.* **83**, 1778-1781 (1989).

32. Laskowski, R. A., MacArthur, M. W., Moss, D. S. & Thornton, J. M. PROCHECK: a program to check the stereochemical quality of protein structures. *J. Appl. Cryst.* **26**, 283-291 (1993).

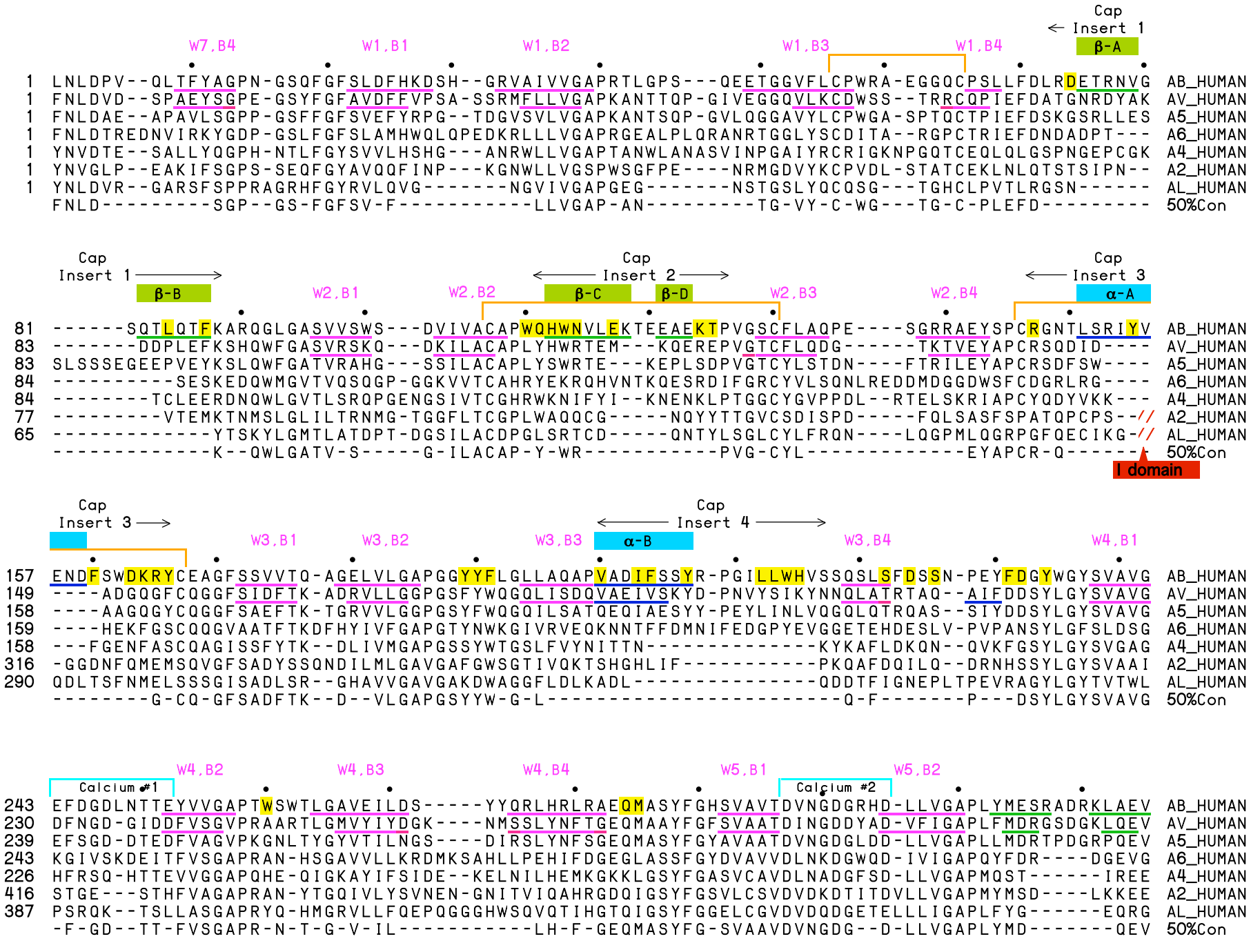
Cap
Insert 1
W7,B4
W1,B1
W1,B2
W1,B3
W1,B4
β-A
1 LNLDPV--QLTFYAGPN-GSQFGFSLDFHKDSH--GRVAIVVGAPRTLGPS---QEETGGVFLCPWRA-EGGQCPSLLFDLRDETRNVG AB_HUMAN
1 FNLDVD--SPAEYSGPE-GSYFGFAVDFFVPSA-SSRMFLLVGAPKANTTQP-GIVEGGQVLKCDWSS--TRRCQPIEFDATGNRDYAK AV_HUMAN
1 FNLDAE--APAVLSGPP-GSFFGFSVEFYRPG--TDGVSVLVGAPKANTSQP-GVLQGGAVYLCPWGA-SPTQCTPIEFDSKGSRLLES A5_HUMAN
1 FNLDTREDNVIRKYGDP-GSLFGFSLAMHWQLQPEDKRLLLVGAPRGEALPLQRANRTGGLYSCDITA--RGPCTRIEFDNDADPT--- A6_HUMAN
1 YNVDTE--SALLYQGPH-NTLFGYSVVLHSHG---ANRWLLVGAPTANWLANASVINPGAIYRCRIGKNPGQTCEQLQLGSPNGEPCGK A4_HUMAN
1 YNVGLP--EAKIFSGPS-SEQFGYAVQQFINP---KGNWLLVGSPWSGFPE----NRMGDVYKCPVDL-STATCEKLNLQTSTSIPN-- A2_HUMAN
1 YNLDVR--GARSFSPPRAGRHFGYRVLQVG-------NGVIVGAPGEG-------NSTGSLYQCQSG---TGHCLPVTLRGSN------ AL_HUMAN
FNLD---------SGP--GS-FGFSV-F-----------LLVGAP-AN---------TG-VY-C-WG---TG-C-PLEFD--------- 50%Con
Cap
Insert 1
β-B
W2,B1
W2,B2
Cap
Insert 2
β-C
β-D
W2,B3
W2,B4
Cap
Insert 3
α-A
81 ------SQTLQTFKARQGLGASVVSWS---DVIVACAPWQHWNVLEKTEEAEKTPVGSCFLAQPE----SGRRAEYSPCRGNTLSRIYV AB_HUMAN
83 -------DDPLEFKSHQWFGASVRSKQ---DKILACAPLYHWRTEM---KQEREPVGTCFLQDG------TKTVEYAPCRSQDID---- AV_HUMAN
83 SLSSSEGEEPVEYKSLQWFGATVRAHG---SSILACAPLYSWRTE---KEPLSDPVGTCYLSTDN----FTRILEYAPCRSDFSW---- A5_HUMAN
84 ----------SESKEDQWMGVTVQSQGP-GGKVVTCAHRYEKRQHVNTKQESRDIFGRCYVLSQNLREDDMDGGDWSFCDGRLRG---- A6_HUMAN
84 --------TCLEERDNQWLGVTLSRQPGENGSIVTCGHRWKNIFYI--KNENKLPTGGCYGVPPDL--RTELSKRIAPCYQDYVKK--- A4_HUMAN
77 ---------VTEMKTNMSLGLILTRNMG-TGGFLTCGPLWAQQCG-----NQYYTTGVCSDISPD-----FQLSASFSPATQPCPS--// A2_HUMAN
65 -------------YTSKYLGMTLATDPT-DGSILACDPGLSRTCD-----QNTYLSGLCYLFRQN----LQGPMLQGRPGFQECIKG-// AL_HUMAN
-------------K--QWLGATV-S-----G-ILACAP-Y-WR----------PVG-CYL-------------EYAPCR-Q------ 50%Con
I domain
Cap
Insert 3
W3,B1
W3,B2
W3,B3
Cap
Insert 4
α-B
W3,B4
W4,B1
157 ENDFSWDKRYCEAGFSSVVTQ-AGELVLGAPGGYYFLGLLAQAPVADIFSSYR-PGILLWHVSSQSLSFDSSN-PEYFDGYWGYSVAVG AB_HUMAN
149 ----ADGQGFCQGGFSIDFTK-ADRVLLGGPGSFYWQGQLISDQVAEIVSKYD-PNVYSIKYNNQLATRTAQ--AIFDDSYLGYSVAVG AV_HUMAN
158 ----AAGQGYCQGGFSAEFTK-TGRVVLGGPGSYFWQGQILSATQEQIAESYY-PEYLINLVQGQLQTRQAS--SIYDDSYLGYSVAVG A5_HUMAN
159 ----HEKFGSCQQGVAATFTKDFHYIVFGAPGTYNWKGIVRVEQKNNTFFDMNIFEDGPYEVGGETEHDESLV-PVPANSYLGFSLDSG A6_HUMAN
158 ---FGENFASCQAGISSFYTK--DLIVMGAPGSSYWTGSLFVYNITTN----------KYKAFLDKQN--QVKFGSYLGYSVGAG A4_HUMAN
316 -GGDNFQMEMSQVGFSADYSSQNDILMLGAVGAFGWSGTIVQKTSHGHLIF----------PKQAFDQILQ--DRNHSSYLGYSVAAI A2_HUMAN
290 QDLTSFNMELSSSGISADLSR--GHAVVGAVGAKDWAGGFLDLKADL----------QDDTFIGNEPLTPEVRAGYLGYTVTWL AL_HUMAN
--------G-CQ-GFSADFTK--D--VLGAPGSYYW-G-L----------Q-F-------P---DSYLGYSVAVG 50%Con
W4,B2
W4,B3
W4,B4
W5,B1
W5,B2
Calcium #1
Calcium #2
243 EFDGDLNTTEYVVGAPTWSWTLGAVEILDS-----YYQRLHRLRAEQMASYFGHSVAVTDVNGDGRHD-LLVGAPLYMESRADRKLAEV AB_HUMAN
230 DFNGD-GIDDFVSGVPRAARTLGMVYIYDGK----NMSSLYNFTGEQMAAYFGFSVAATDINGDDYAD-VFIGAPLFMDRGSDGKLQEV AV_HUMAN
239 EFSGD-DTEDFVAGVPKGNLTYGYVTILNGS----DIRSLYNFSGEQMASYFGYAVAATDVNGDGLDD-LLVGAPLLMDRTPDGRPQEV A5_HUMAN
243 KGIVSKDEITFVSGAPRAN-HSGAVVLLKRDMKSAHLLPEHIFDGEGLASSFGYDVAVVDLNKDGWQD-IVIGAPQYFDR----DGEVG A6_HUMAN
226 HFRSQ-HTTEVVGGAPQHE-QIGKAYIFSIDE--KELNILHEMKGKKLGSYFGASVCAVDLNADGFSD-LLVGAPMQST------IREE A4_HUMAN
416 STGE---STHFVAGAPRAN-YTGQIVLYSVNEN-GNITVIQAHRGDQIGSYFGSVLCSVDVDKDTITDVLLVGAPMYMSD----LKKEE A2_HUMAN
387 PSRQK--TSLLASGAPRYQ-HMGRVLLFQEPQGGGHWSQVQTIHGTQIGSYFGGELCGVDVDQDGETELLLIGAPLFYG------EQRG AL_HUMAN
-F-GD--TT-FVSGAPR-N-T-G-V-IL----------LH-F-GEQMASYFG-SVAAVDVNGDG--D-LLVGAPLYMD-------QEV 50%Con

```
                W5,B3                W5,B4                W6,B1                W6,B2                W6,B3        W6,B4
                   •                    •                    •          Calcium #3                •            •            •
326  GRVYLFLQPRGPHALGAPSLLLTGTQL--YGRFGSAIAPLGDLDRDGYNDIAVAAPYGGPSGRGQVLVFLGQSEGLRSRPSQVLDSPFP  AB_HUMAN
313  GQVSVSLYRAS-GDFQT--TKLNGFEV--FARFGSAIAPLGDLDQDGFNDIAIAAPYGGEDKKGIVYIFNGRSTGLNAVPSQILEGQWA  AV_HUMAN
322  GRVYVYLQHPA-GIEPTPTLTLTGHDE--FGRFGSSLTPLGDLDQDGYNDVAIGAPFGGETQQGVVFVFPGGPGGLGSKPSQVLQPLWA  A5_HUMAN
326  GAVYVYMNQQG-RWNNVKPIRLNGTKD---SMFGIAVKNIGDINQDGYPDIAVGAPYD---DLGKVFIYHGSANGINTKPTQVLKGIS-  A6_HUMAN
304  GRVFVYINSGSGAVMNAMETNLVGSDKY-AARFGESIVNLGDIDNDGFEDVAIGAPQED-DLQGAIYIYNGRADGISSTFSQRIEGLQI  A4_HUMAN
496  GRVYLFTIKKG--ILGQH-QFLEGPEGIENTRFGSAIAALSDINMDGFNDVIVGSPLEN-QNSGAVYIYNGHQGTIRTKYSQKILGSDG  A2_HUMAN
467  GRVFIYQRRQL--GFEEV-SELQGDPGYPLGRFGEAITALTDINGDGLVDVAVGAPLE---EQGAVYIFNGRHGGLSPQPSQRIEGTQV  AL_HUMAN
     GRVYVYL---G----------L-G------GRFGSAIAPLGDIDQDGYNDVAVGAPYE----QGAVYIFNGR-GGL-S-PSQVLEG---  50%Con

                W7,B1                W7,B2                W7,B3
                   •          Calcium #4                •            •
413  T----GSAFGFSLRGAVDIDDNGYPDLIVGAYGANQVAVYRAQP  AB_HUMAN
397  ARSM-PPSFGYSMKGATDIDKNGYPDLIVGAFGVDRAILYRARP  AV_HUMAN
408  ASHT-PDFFGSALRGGRDLDGNGYPDLIVGSFGVDKAVVYRGRP  A5_HUMAN
407  ------PYFGYSIAGNMDLDRNSYPDVAVGSL-SDSVTIFRSRP  A6_HUMAN
391  SK-S-LSMFGQSISGQIDADNNGYVDVAVGAFRSDSAVLLRTRP  A4_HUMAN
581  AFRSHLQYFGRSLDGYGDLNGDSITDVSIGAFG--QVVQLWSQS  A2_HUMAN
550  LS-G-IQWFGRSIHGVKDLEGDGLADVAVGAES--QMIVLSSRP  AL_HUMAN
     --------FG-SL-G--DLDGNGYPDVIVGAFG--QVVVYRSRP  50%Con
```

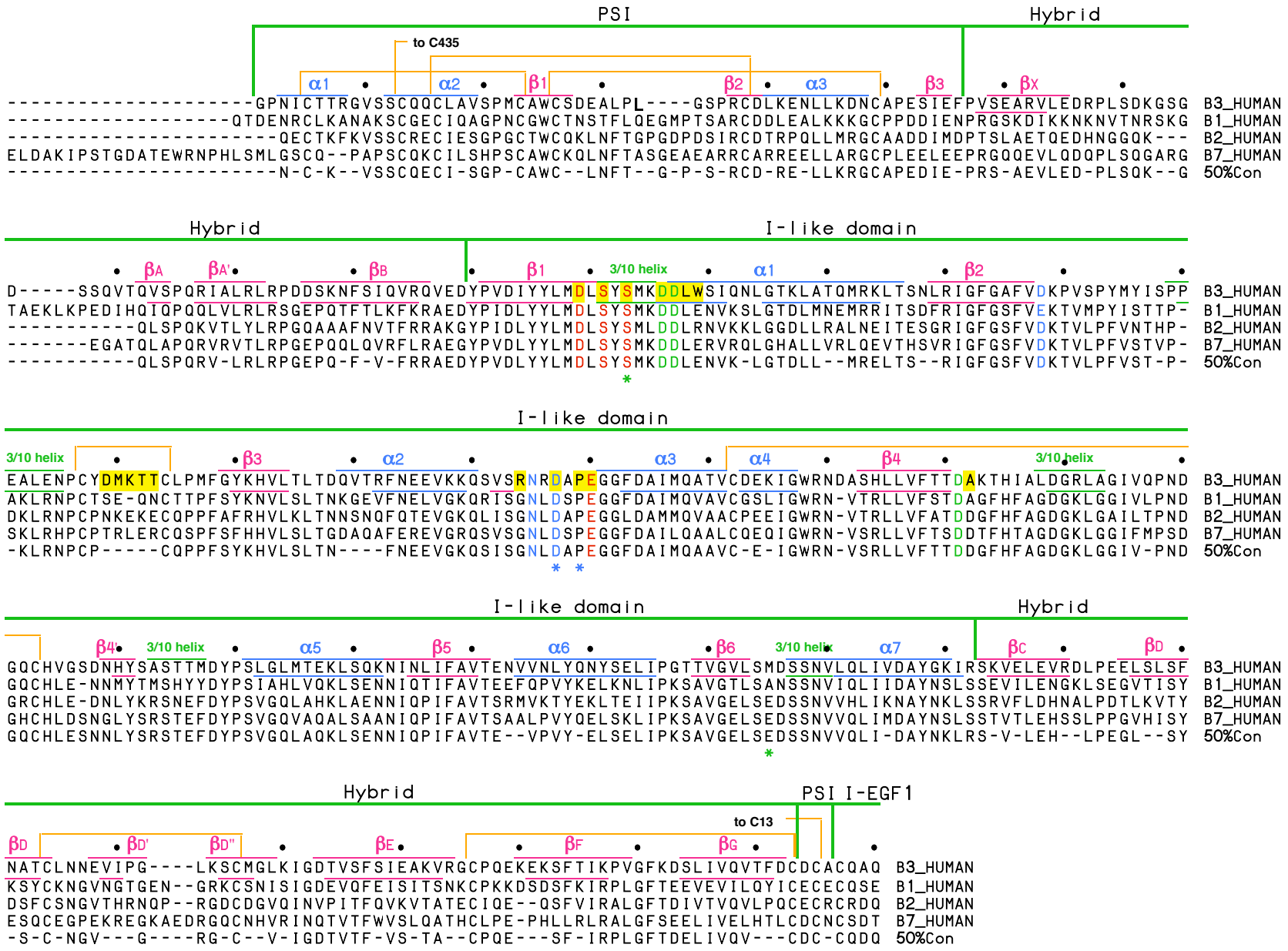
PSI
Hybrid
to C435
α1 α2 β1 β2 α3 β3 βX
1 ----------GPNICTTRGVSSCQQCLAVSPMCAWCSDEALPL----GSPRCDLKENLLKDNCAPESIEFPVSEARVLEDRPLSDKGSG B3_HUMAN
1 ----------QTDENRCLKANAKSCGECIQAGPNCGWCTNSTFLQEGMPTSARCDDLEALKKKGCPPDDIENPRGSKDIKKNKNVTNRSKG B1_HUMAN
1 ----------QECTKFKVSSCRECIESGPGCTWCQKLNFTGPGDPDSIRCDTRPQLLMRGCAADDIMDPTSLAETQEDHNGGQK--- B2_HUMAN
1 ELDAKIPSTGDATEWRNPHLSMLGSCQ--PAPSCQKCILSHPSCAWCKQLNFTASGEAEARRCARREELLARGCPLEELEEPRGQQEVLQDQPLSQGARG B7_HUMAN
----------N-C-K--VSSCQECI-SGP-CAWC--LNFT--G-P-S-RCD-RE-LLKRGCAPEDIE-PRS-AEVLED-PLSQK--G 50%Con
Hybrid
I-like domain
βA βA' βB β1 3/10 helix α1 β2
76 D-----SSQVTQVSPQRIALRLRPDDSKNFSIQVRQVEDYPVDIYYLMDLSYSMKDDLWSIQNLGTKLATQMRKLTSNLRIGFGAFVDKPVSPYMYISPP B3_HUMAN
82 TAEKLKPEDIHQIQPQQLVLRLRSGEPQTFTLKFKRAEDYPIDLYYLMDLSYSMKDDLENVKSLGTDLMNEMRRITSDFRIGFGSFVEKTVMPYISTTP- B1_HUMAN
75 ----------QLSPQKVTLYLRPGQAAAFNVTFRRAKGYPIDLYYLMDLSYSMLDDLRNVKKLGGDLLRALNEITESGRIGFGSFVDKTVLPFVNTHP- B2_HUMAN
99 -------EGATQLAPQRVRVTLRPGEPQQLQVRFLRAEGYPVDLYYLMDLSYSMKDDLERVRQLGHALLVRLQEVTHSVRIGFGSFVDKTVLPFVSTVP- B7_HUMAN
----------QLSPQRV-LRLRPGEPQ-F-V-FRRAEDYPVDLYYLMDLSYSMKDDLENVK-LGTDLL--MRELTS--RIGFGSFVDKTVLPFVST-P- 50%Con
*
I-like domain
3/10 helix β3 α2 α3 α4 β4 3/10 helix
171 EALENPCYDMKTTCLPMFGYKHVLTLTDQVTRFNEEVKKQSVSRNRDAPEGGFDAIMQATVCDEKIGWRNDASHLLVFTTDAKTHIALDGRLAGIVQPND B3_HUMAN
181 AKLRNPCTSE-QNCTTPFSYKNVLSLTNKGEVFNELVGKQRISGNLDSPEGGFDAIMQVAVCGSLIGWRN-VTRLLVFSTDAGFHFAGDGKLGGIVLPND B1_HUMAN
163 DKLRNPCPNKEKECQPPFAFRHVLKLTNNSNQFQTEVGKQLISGNLDAPEGGLDAMMQVAACPEEIGWRN-VTRLLVFATDDGFHFAGDGKLGAILTPND B2_HUMAN
191 SKLRHPCPTRLERCQSPFSFHHVLSLTGDAQAFEREVGRQSVSGNLDSPEGGFDAILQAALCQEQIGWRN-VSRLLVFTSDDTFHTAGDGKLGGIFMPSD B7_HUMAN
-KLRNPCP-----CQPPFSYKHVLSLTN----FNEEVGKQSISGNLDAPEGGFDAIMQAAVC-E-IGWRN-VSRLLVFTTDDGFHFAGDGKLGGIV-PND 50%Con
* *
I-like domain
Hybrid
β4 3/10 helix α5 β5 α6 β6 3/10 helix α7 βC βD
271 GQCHVGSDNHYSASTTMDYPSLGLMTEKLSQKNINLIFAVTENVVNLYQNYSELIPGTTVGVLSMDSSNVLQLIVDAYGKIRSKVELEVRDLPEELSLSF B3_HUMAN
279 GQCHLE-NNMYTMSHYYDYPSIAHLVQKLSENNIQTIFAVTEEFQPVYKELKNLIPKSAVGTLSANSSNVIQLIIDAYNSLSSEVILENGKLSEGVTISY B1_HUMAN
262 GRCHLE-DNLYKRSNEFDYPSVGQLAHKLAENNIQPIFAVTSRMVKTYEKLTEIIPKSAVGELSEDSSNVVHLIKNAYNKLSSRVFLDHNALPDTLKVTY B2_HUMAN
290 GHCHLDSNGLYSRSTEFDYPSVGQVAQALSAANIQPIFAVTSAALPVYQELSKLIPKSAVGELSEDSSNVVQLIMDAYNSLSSTVTLEHSSLPPGVHISY B7_HUMAN
GQCHLESNNLYSRSTEFDYPSVGQLAQKLSENNIQPIFAVTE--VPVY-ELSELIPKSAVGELSEDSSNVVQLI-DAYNKLRS-V-LEH--LPEGL--SY 50%Con
*
Hybrid
PSI I-EGF1
to C13
βD βD' βD" βE βF βG
371 NATCLNNEVIPG----LKSCMGLKIGDTVSFSIEAKVRGCPQEKEKSFTIKPVGFKDSLIVQVTFDCDCACQAQ B3_HUMAN
378 KSYCKNGVNGTGEN--GRKCSNISIGDEVQFEISITSNKCPKKDSDSFKIRPLGFTEEVEVILQYICECECQSE B1_HUMAN
361 DSFCSNGVTHRNQP--RGDCDGVQINVPITFQVKVTATECIQE--QSFVIRALGFTDIVTVQVLPQCECRCRDQ B2_HUMAN
390 ESQCEGPEKREGKAEDRGQCNHVRINQTVTFWVSLQATHCLPE-PHLLRLRALGFSEELIVELHTLCDCNCSDT B7_HUMAN
-S-C-NGV---G----RG-C--V-IGDTVTF-VS-TA--CPQE---SF-IRPLGFTDELIVQV---CDC-CQDQ 50%Con

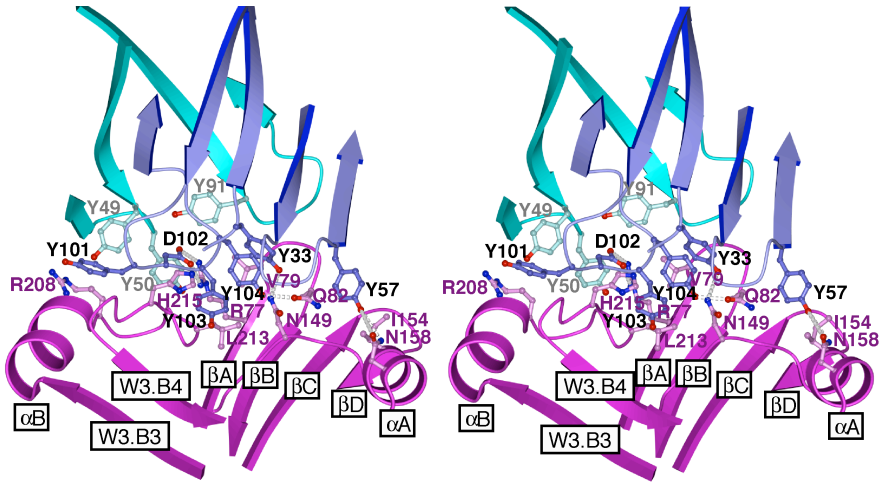
Y91
Y49
Y101
D102
Y33
R208
Y50
V79
Y104
Q82
Y57
H215
B77
Y103
N149
I154
L213
N158
W3.B4
βA
βB
βC
βD
αB
αA
W3.B3
Y91
Y49
Y101
D102
Y33
R208
Y50
V79
Y104
Q82
Y57
H215
B77
Y103
N149
I154
L213
N158
W3.B4
βA
βB
βC
βD
αB
αA
W3.B3

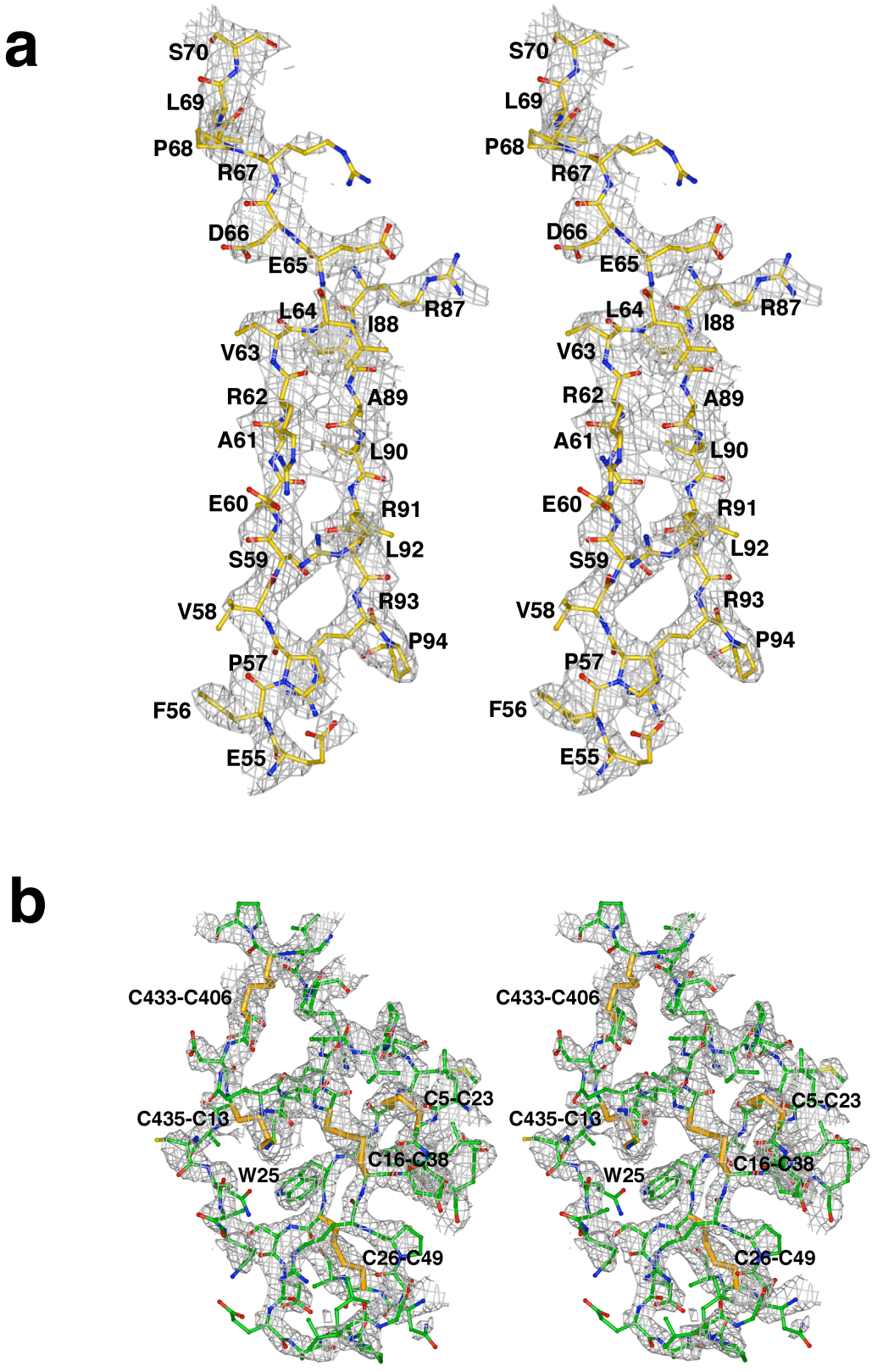
a
S70
L69
P68
R67
D66
E65
L64
I88
R87
V63
R62
A89
A61
L90
E60
R91
S59
L92
V58
R93
P94
P57
F56
E55
S70
L69
P68
R67
D66
E65
L64
I88
R87
V63
R62
A89
A61
L90
E60
R91
S59
L92
V58
R93
P94
P57
F56
E55
b
C433-C406
C5-C23
C435-C13
C16-C38
W25
C26-C49
C433-C406
C5-C23
C435-C13
C16-C38
W25
C26-C49

Xiao et al., S. 3

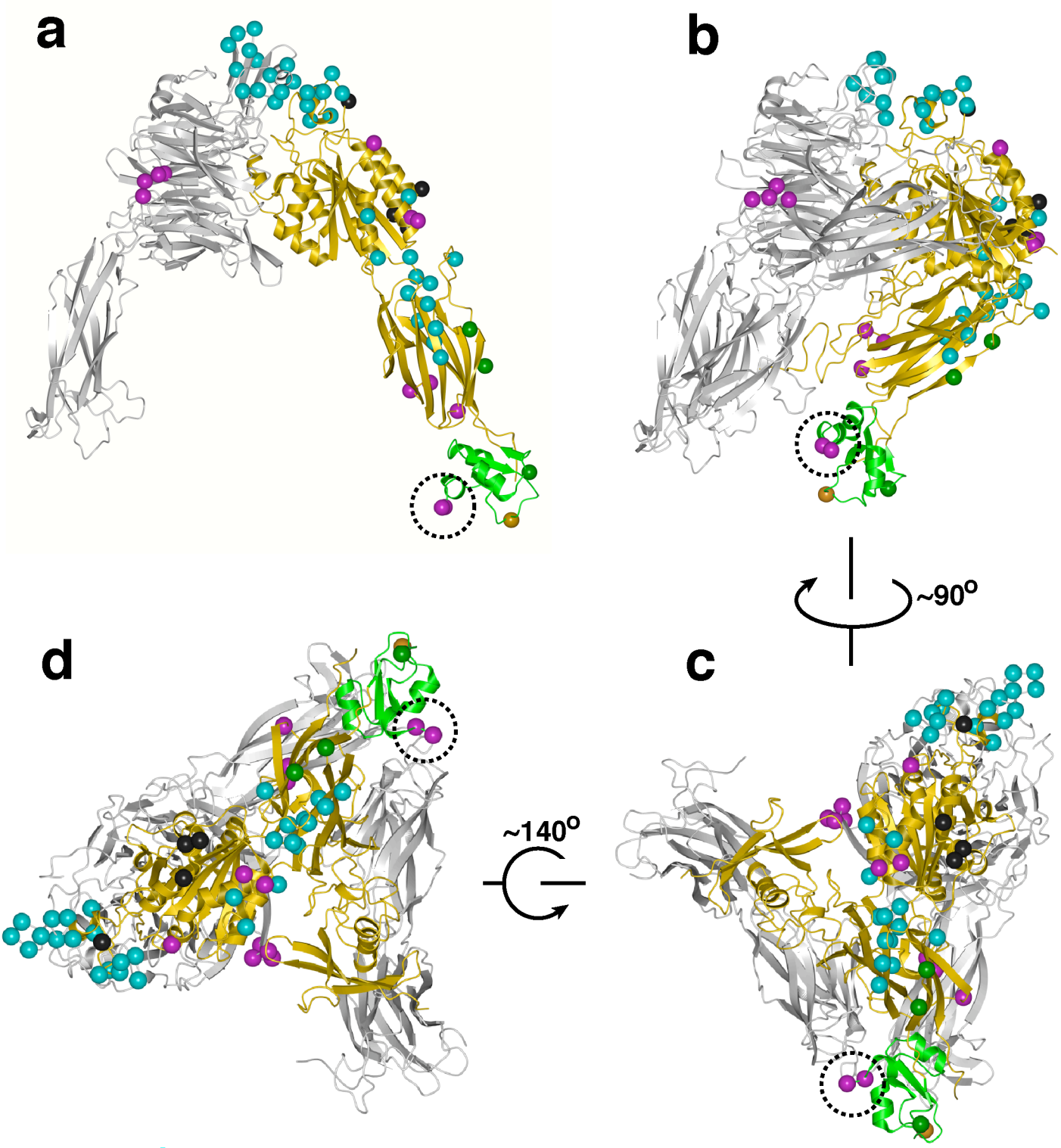
a
b
~90°
d
c
~140°
Inhibitory mAb epitopes
Activating mAb epitopes
Epitopes for both types of mAbs
Allo-antigen epitope
Drug-dependent epitope

Xiao et al., S.4